LASER INTERFEROMETER GRAVITATIONAL WAVE OBSERVATORY
- LIGO -
CALIFORNIA INSTITUTE OF TECHNOLOGY
MASSACHUSETTS INSTITUTE OF TECHNOLOGY

Document Type	**LIGO-T980009-01 - D**	3/17/98

Input Optics
Final Design

Rana Adhikari, Aaron Bengston, Yasha Buchler, Tom Delker,
David Reitze, Qi-Ze Shu, David Tanner, Sanichiro Yoshida

Distribution of this document:

IOO Design Review Board

This is an internal working note
of the LIGO Project.

California Institute of Technology
LIGO Project - MS 51-33
Pasadena CA 91125
Phone (818) 395-2129
Fax (818) 304-9834
E-mail: info@ligo.caltech.edu

Massachusetts Institute of Technology
LIGO Project - MS 20B-145
Cambridge, MA 01239
Phone (617) 253-4824
Fax (617) 253-7014
E-mail: info@ligo.mit.edu

WWW: http://www.ligo.caltech.edu/

j

TABLE OF CONTENTS

1 INTRODUCTION

1.1. Purpose

This document along with supporting analysis documents presents the final design for the LIGO Input Optics. The design information in this document supersede that presented in the IOO Preliminary and Conceptual Designs and is intended to present a detailed final design for the LIGO Input Optics Subsystem which conform to the *Input Optics Design Requirements*, LIGO-T960093-00-D. This document is intended for the LIGO Detector Team.

1.2. Scope

The IOO provides for the conditioning of the laser light after the PSL and before the IFO input, and for the disposition of the IFO reflected light to the LSC and ASC subsystems. It includes RF phase modulation of the light for the generation of resonant and non-resonant sidebands; mode-matching, lock acquisition and operation of the mode cleaner; mode matching of the light to the IFO; beam steering into the IFO; and diagnostic beam pick-offs for the LSC/ASC subsystems.

1.2.1. IOO Subsystems

The Input / Output (IOO) subsystem layout consists of the following units, schematically shown in Figure 1:

- RF modulation
- Steering and conditioning optics
- Mode cleaner and controls
- IFO mode matching and beam pointing
- IFO signal extraction for ASC
- Signal extraction for PSL intensity control

Figure 1: IOO Subsystem Components

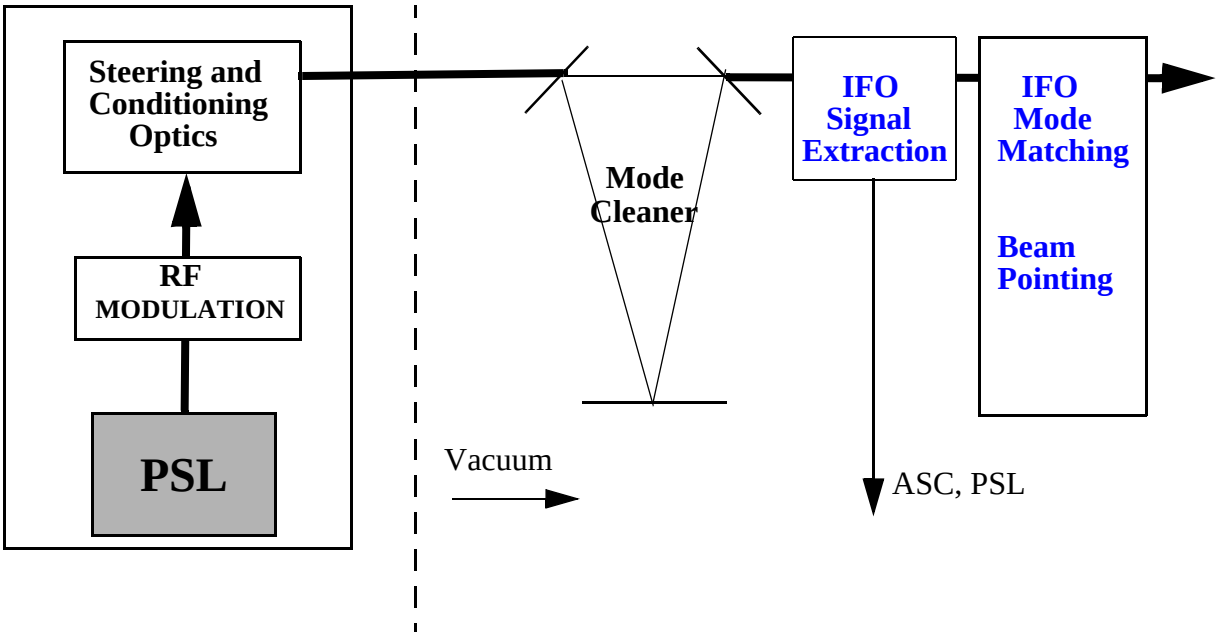

1.3. Document Organization

1.3.1. Definitions

- TEM_{00} Gaussian beam: A beam of electromagnetic radiation, in which the transverse electric field varies as $E = E_0 e^{-r^2/w^2}$, where w is the beam spot size and E_0 is the electric field strength at r=0.
- Spot size: The characteristic size for Gaussian laser beams, defined as the distance (radius) at which the electric field drops to $1/e$ times the maximum value, E_0 (at $r = 0$).
- Beam Divergence Half Angle - The far field angular divergence θ_d of a Gaussian beam is defined in terms of the half angle formula $\theta_d/2 = \frac{\lambda}{\pi w_0}$
- Modulation index Γ: The application of RF sidebands using an EOM results in a output field $E_{mod} = E_{in} e^{-i\omega t - i\Gamma\cos\Omega t}$ where ω and Ω are the carrier and modulation frequencies and E_{in} is the input field amplitude.

1.3.2. Acronyms

AM	Amplitude Modulation
ASC	Alignment Sensing / Control (detector subsystem)
BS	Beamsplitter (optical component)
CDS	Control and Data System (detector subsystem)
CIT	California Institute of Technology
COC	Core Optics Components (detector subsystem)
COS	Core Optics Support (detector subsystem)
DC	Direct Current (steady state - low frequency)
EOM	Electro-Optic Modulator (optical hardware)
ETM	End Test Mass (optical component)
FI	Faraday Isolator (optical component)
FR	Faraday Rotator (optical component)
GW	Gravitational Wave
HAM	Horizontal Access Module
HWP	Half-Wave Plate (optical hardware)
IFO	LIGO Interferometer
IOO	Input Optics (detector subsystem, formerly named Input / Output Optics)
ITM	Input Test Mass (optical component)
LHAM	Horizontal Access Module at Louisiana Site
LIGO	Laser Interferometer Gravitational-Wave Observatory
LSC	Length Sensing / Control (detector subsystem)
LOS	Large Optic Suspension
LVEA	Laser and Vacuum Equipment Area (of the LIGO observatories)
MC	Mode Cleaner
MCM	Mode Cleaner Mirror
MIT	Massachusetts Institute of Technology
MMT	IFO Mode Matching Telescope
MZ	Mach-Zender Interferometer
Nd:YAG	Neodynium doped Yttrium Aluminum Garnet (laser gain medium)
PDD	Preliminary Design Document
PDH	Pound-Drever-Hall (reflection locking technique)
PM	Phase Modulation
PSL	Pre-Stabilized Laser (detector subsystem)
PZT	Piezo-electric Transducer (mechanical hardware)
RC	Radius of Curvature of a Reflective Mirror
RF	Radio Frequency
RM	Recycling Mirror
SAH	Sensor Actuator Heads
SEI	Seismic Isolation
SOS	Small Optic Suspension
TGG	Terbium-Gallium-Garnet (optical material used in Faraday Isolators)
TFP	Thin Film Polarizer (optical hardware)
UF	University of Florida
WFS	Wave Front Sensors

WHAM Horizontal Access Module at Washington Site

1.3.3. Relevant Documents

1.3.3.1 LIGO Documents

Core Optics Support Preliminary Design, Mike Smith, LIGO-T980010-D
Input Optics Design Requirements Document, J. Camp, D. Reitze, and D. Tanner, *LIGO-T960093-00-D*
Input Optics Conceptual Design, J. Camp, D. Reitze, and D. Tanner, *LIGO-T960170-00-D*
Input Optics Preliminary Design, Rana Adhikari, Tom Delker, David Reitze, Qi-Ze Shu, David Tanner, Sanichiro Yoshida, *LIGO-T9701xx-00-D*
Mode Cleaner Length/Frequency Control Design, P. Fritschel, N. Mavalvala, D. Ouimette, LIGO-T970218-01-D
Absorption in the Core Optics and LIGO Sensitivity, J. Camp and B. Kells, LIGO-T970xxx-00-D
ASC Initial Alignment, K. Mason and M. Zucker, *LIGO-T970151-00-D*
Alignment Sensing/Control Design Requirement Document, P. Fritschel, *LIGO-T952007-03-I*
Alignment Sensing/Control Preliminary Design, P. Fritschel, G. Gonzalez, D. Sigg, M. Zucker, *LIGO-T970060-00-D*
Detector Subsystems Requirements, D. Shoemaker, *LIGO-E960112-05-D*
Design Considerations for LIGO Mode-Matching Telescopes, T. Delker, R. Adhikari, S Yoshida, and D. Reitze, *LIGO-T970143-00-D*
Effects of Stray Magnetic Fields Generated by Faraday Isolators on Suspended Optical Components, S. Yoshida, R. Adhikari, and D. Reitze, *LIGO-T970149-00-D*
Frequency Stabilization: Servo Configuration & Subsystem Interface Specification, P. Fritschel, *LIGO-T970088-00-D*
Impact of Non-resonant Sidebands on Length Sensing Signals, J. Camp, *LIGO-T970097-00-D*
(Infrared) Pre-Stabilized Laser (PSL) Conceptual Design, R. Abbott, P. King, R.Savage, S Seel, *LIGO-T970087-00-D*
Initial length precision of LIGO suspended cavities, J. Camp, *LIGO-T960181.*
LIGO cavity lengths and modulation frequencies, D.B. Tanner, *LIGO-T-970xxx-03-D*
MIT Meeting on RF Modulation, David Shoemaker, LIGO-T970155-00-D
Modal Model Update 4: Mode-Matching, D. Sigg, *LIGO-T960116-00-D*
Modal Model Update 6: Mode Cleaner, D. Sigg, *LIGO-T960118-00-D*
Mode Cleaner Noise Sources, J. Camp, *LIGO-T960165-00-D*
Mode Matching Wavefront Sensor, Qi-Ze Shu, Rana Adhikari, David Reitze, David Tanner, *LIGO-T980021-00-D*
Proposed initial detector MC and RC baseline lengths, M. Zucker and P. Fritschel, *LIGO-T960122-00-I.*
Recycling cavity and mode cleaner baseline dimensions, D. Coyne, *LIGO-T970068-00-D*
Seismic Isolation Design Requirements, Fred Raab, *LIGO T960065-03-D*
Small Optics Suspensions Final Design, S. Kawamura, *LIGO-T970135-02-D*

1.3.3.2 Non-LIGO Documents

Heating by Optical Absorption and the Performance of Gravitational Wave Detectors, W.Winkler, K. Danzmann, A. Ruediger, and R. Schilling, Phys Rev A, 44, 7022.

Optical mode cleaner with suspended mirrors, A. Araya, N. Mio, K. Tsubono, K. Suehiro, S. Telada, M. Ohashi, and M. Fujimoto, Appl. Opt. **39**, 1446 (1977).

The response of a Fabry-Perot optical cavity to phase modulation sidebands for use in electro-optic control systems, K.D. Skelton, and K.A. Strain, Applied Optics Lasers, *in press.*

Alignment of Resonant Optical Cavities, D. Anderson, Appl. Opt. **23**, 2944 (1984).

2 OVERVIEW OF THE FINAL DESIGN

2.1. Design Status

The design for the IOO is substantially complete. All of the main IOO subsystems have been designed to meet the requirements set forth in *Input Optics Design Requirements Document*. Several parts are already in production or completed. These include:

- The SOSs and spares for the 2 km IFO has been completed. The SOS for the WA4k and LA4k IFOs are underway.
- All of the custom optics for the IOO have been designed and ordered and are currently in production. Mirror blanks have been received from Corning Corporation and are currently being polished by General Optics. Coating runs have been scheduled with Research Electro-optics.

2.2. Design Changes

Since the IOO preliminary design, the following design changes have taken place in the IOO subsystems:

2.2.1. Assignment of the Mode Cleaner Length and Alignment Control Design to the ISC group

The development and integration of the mode cleaner length and alignment controls within the global LIGO control hierarchy has been transferred from the IOO group to the ISC group. This decision was based on a number of factors:

- The complexity of the control topology and hierarchy for the LIGO interferometers mandated that the design and integration of the MC length controls be coordinated within the design of the IFO controls. The assignment of the MC length controls to ISC makes sense from an integration standpoint.
- The ISC group are the control ‘experts’ within LIGO and thus the reassignment makes sense from the standpoint of efficient allocation of manpower.
- The design of the ASC for the MC is a slight modification of that done for the COC.[1] Again, from an efficiency standpoint, ASC was better suited to this task.

While the design is carried out by ISC, the fabrication and implementation of the MC LSC and ASC components remain in the IOO.

2.2.2. Development of a Mode Matching Sensor Based on Wavefront Sensing

One of the tasks identified in the IOO PDR was the ability to accurately measure the amount of mode-matched TEM_{00} power in the COC in such a way that correct adjustments to the MMT could be predicted from the measurement. We have designed a WFS sensing system[2] similar to

1. *Modal Model Update 6: Mode Cleaner,* D. Sigg, *LIGO-T960118-00-D*

alignment sensing system for the COC for measuring the amount of the higher order Hermite LaGuerre (cylindrical) modes (or alternatively, the amount of beam waist position and waist size mismatch). The mode mismatch is measured by dithering the second telescope mirror (MMT2) and monitoring the error signal carried by the reflected carrier and sideband light using two specially designed cylindrically symmetric ("bull's eye") photodiodes.

We had originally intended to have a prototype mode matching measurement made by the time of the IOO FDR. However, the fabrication of the custom designed four element photodiode (see Section 9) by the Advanced Photonix Corporation had a 16 week production lead time and is not scheduled for delivery to UF until April 17, 1998. Unfortunately, not having the photodiode has prevented us from prototyping the measurement. This will commence when we receive the photodiode and will be complete by the installation of the ISC diagnostics. Nevertheless, in this document, we present a complete design for the IFO mode matching measurement.

2.2.3. Removal of Redundant Diagnostics from the PSL/IOO Table

In the IOO preliminary design, there were a number of diagnostic functions which duplicated those from other subsystems or became extraneous during the IOO final design. These include:

- laser power monitoring (performed in the PSL).
- monitoring of transmitted mode in the optical spectrum analyzer.

2.2.4. Removal of Optical Levers from MMT1 and MMT2 optics

The IOO PDR presented an optical lever system for maintaining the positioning of the beams on the MMT mirrors. Based on the expected amount of stack drift and tolerance of the MMT design to small changes in angle and separation (see Appendix X), optical levering of MMT1 and MMT2 is not necessary and has been eliminated from the design.

2.2.5. Respecification of MMT Wedge Angles and Radii of Curvature

Since the PDR, changes have been made to the wedge angles of the MC and MMT optics to provide conformity with SOS and LOS1 designs. In addition, the 4 km MMT3 telescope has been redesigned to allow for the same radii of curvature of MMT3 for both 2 km and 4 km IFOs. This design decision eliminated the need for polishing two different large optics radii of curvature, thus economizing and streamlining the polishing process.

2.3. Detailed Components Specification

A complete list of IOO components can be found in LIGO X9800xx-00.

2. *Modal Model Update 4: Mode-Matching*, D. Sigg, *LIGO-T960116-00-D; Mode Matching Wavefront Sensor*, Qi-Ze Shu, Rana Adhikari, David Reitze, David Tanner, *LIGO-LIGO-T980021-00-D*

3 SUBSYSTEM INTERFACES

By and large, optical, mechanical, and electrical interfaces have remained the same as those presented in the IOO PDD. The following constitutes a complete list of interfaces between the IOO and other LIGO subsystems.

3.1. PSL

The PSL delivers the main LIGO laser beam to the IOO and receives a diagnostic beam for intensity stabilization after the IOO MC.

3.1.1. Optical Interfaces

3.1.1.1 Main Beam

The optical interfaces between the PSL and IOO are given in Table 1 and Table 2. The PSL/IOO optical table local coordinate system is defined in Figure 2. The IOT1,7 coordinate systems are defined in Figure 3.

Table 1: IOO/PSL Optical Interfaces for the 2 km IFO

Optical Interface	*Interface Description*	*Value/Tolerance*	*Coordinates*
Main Beam	Location of Handoff of Main Beam from PSL to IOO subsystems	(72.5 $in \pm 0.25 in$, 12.5 $in \pm 0.25 in$, 3.0 $in \pm 0.1 in$)	PSLWA2K local coordinate system (2 km PSL/IOO table)
	Waist Size	0.5 mm $\pm 0.1 mm$	
	Waist Position Uncertainty	$\pm 5 cm$	Measured from PSL/IOO Interface Location
	Polarization	S pol.	
	Polarization Ratio	>100:1	
	Beam Power in TEM_{00}	8.5 W	
	Beam Power in Higher Order Modes	< 1 W	
PSL Intensity Stabilization Pickoff	Location of Handoff of Diagnostic Intensity Stabilization Beam from the IOO to the PSL	(13.75 $in \pm 0.25 in$, 5.4 $in \pm 0.25 in$, 3" $in \pm 0.1 in$) (PSL Intensity Stabilization Photodiode)	IOT7 local coordinate system (2 km IOO ISC table)

Table 1: IOO/PSL Optical Interfaces for the 2 km IFO

Optical Interface	*Interface Description*	*Value/Tolerance*	*Coordinates*
	Beam Size at Interface	$2mm \pm 0.2mm$	
	Beam Divergence Half Angle	0.3 mrad (converging)	
	Beam Power at Interface	25 mW	

Table 2: IOO/PSL Optical Interfaces for the 4 km IFO

Optical Interface	*Interface Description*	*Value/Tolerance*	*Coordinates*
Main Beam	Location of Handoff of Main Beam from PSL to IOO sub-systems	($72.5\ in \pm 0.25in$, $12.5\ in \pm 0.25in$, $3.0\ in \pm 0.1in$)	4 km PSL/IOO table local coordinate system
	Waist Size	0.5 mm $\pm 0.1mm$	
	Waist Position	$\pm 5cm$	Measured from Interface Location
	Polarization	S pol.	
	Polarization Ratio	>100:1	
	Beam Power in TEM_{00}	8.5 W	
	Beam Power in Higher Order Modes	< 1 W	
PSL Intensity Stabilization Pickoff	Location of Handoff of Diagnostic Intensity Stabilization Beam from the IOO to the PSL	($13.75\ in \pm 0.25in$, $5.4\ in \pm 0.25in$, $3"\ in \pm 0.1in$) (PSL Intensity Stabilization Photodiode	IOT1 local coordinate system (2 km IOO ISC table)
	Beam Size at Interface	$2mm \pm 0.2mm$	
	Beam Divergence Half Angle	0.3 mrad (converging)	
	Beam Power at Interface	25 mW	

Figure 2: Shared PSL/IOO Optical Table for 2 km, 4 km IFO

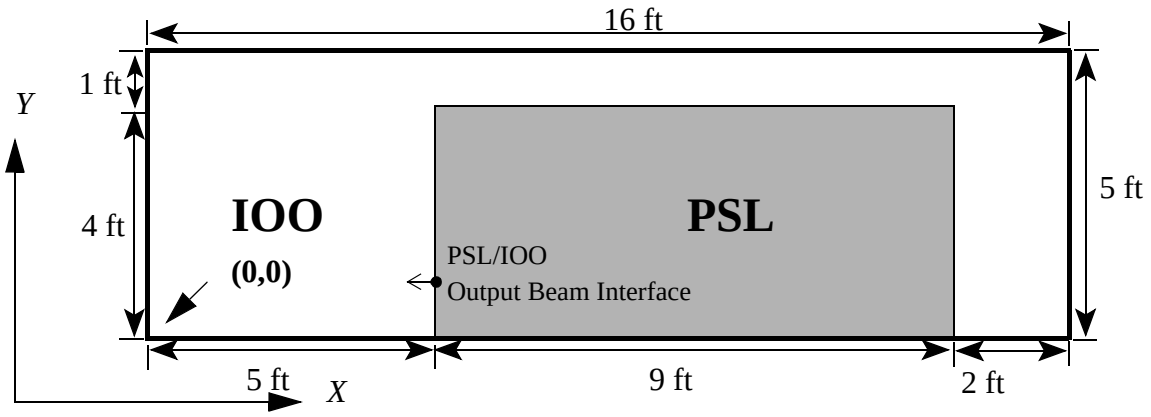

Figure 3: IOT1,7 Optical Table Coordinate System

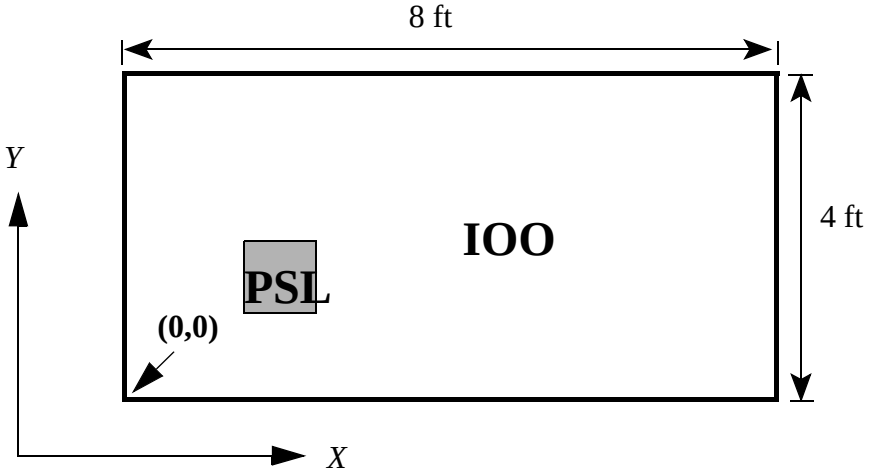

3.1.2. Mechanical

The IOO shares an optical table with the PSL (PSL/IOO table). Figure 2 shows the allocation of table area for each subsystem. The optical table and the physical enclosure surrounding the table (for controlling acoustic noise, air currents, dust, and thermal variations) are the responsibility of the PSL subsystem. IOO is responsible for the positioning of the PSL/IOO table and the vibration isolation of the table from the LVEA floor. A Newport RS-4000 optical table and four HH1 static Newport table legs have been selected for the PSL/IOO table.

The IOO also provides space on IOT1,7 for location of the PSL Intensity Stabilization Photo-diode. The allocation of IOT1,7 table area is shown in Figure 3. IOT1,7 are ‘owned’ by ISC but occupied by the mode cleaner length and alignment sensing systems.

Table 3: IOO/PSL Mechanical Interfaces for the 2,4 km IFO

Mechanical Interface	*Interface Description*	*Value/Tolerance*	*Coordinates*
2 km PSL/IOO Optical Table: PSL-WA2k	Table location (measured at center of table surface)	(-136 *in* ±0.25*in* ,0 *in* ±0.25*in* , 35.0 +0.25, -0.0 *in*);	Ham Center-line
4 km PSL/IOO Optical Table: PSL-WA4k	Table location (measured at center of table surface)	(-136 *in* ±0.25*in* ,0 *in* ±0.25*in* , 35.0 +0.25, -0.0 *in*);	Ham Center-line
4 km PSL/IOO Optical Table: PSL-LA4k	Table location (measured at center of table surface)	(-136 *in* ±0.25*in* ,0 *in* ±0.25*in* , 35.0 +0.25, -0.0 *in*);	Ham Center-line

3.2. COC

The IOO delivers the main beam to the COC at the recycling mirror.

3.2.1. Optical

Table 4 and Table 5 display the IOO/COC optical interfaces for the 2 km and 4 km IFO.

Table 4: IOO/COC Optical Interfaces for the 2 km IFO

Optical Interface	*Interface Description*	*Value/Tolerance*	*Coordinates*
Main Beam	Location of Handoff of laser beam from IOO to COC sub-systems	(12.2786 m±0.5*mm*, 9.0597 m±0.5*mm*, 0.045 m±0.5*mm*)	Global LIGO Coordinate System
	Propagation Direction	(-1.000000, -0.00013700, 0.00000000)	Direction Cosines
	Beam Size (1/e field radius)	3.22 cm	
	Beam Divergence Half Angle	11.5 μrad	
	Polarization	P pol.	

Optical Interface	*Interface Description*	*Value/Tolerance*	*Coordinates*
	Polarization Ratio	>100:1	
	Beam Power in TEM_{00}	> 6 W	
	Beam Power in Higher Order Modes	$< 4 \times 10^{-5}$ W	

Table 5: IOO/COC Optical Interfaces for the 4 km IF

Optical Interface	*Interface Description*	*Value/Tolerance*	*Coordinates*
Main Beam	Location of Handoff of laser beam from IOO to COC sub-systems	(-4.6906 m±0.5*mm*, 0.212 m±0.5*mm*, 0.0278 m±0.5*mm*)	Global LIGO Coordinates
	Propagation Direction	(1.000000, 0.0013673, 0.0000000)	Direction Cosines
	Beam Size (1/e field radius)	3.64 cm	
	Beam Divergence Half Angle	10.7 μrad	
	Polarization	P pol.	
	Polarization Ratio	>100:1	
	Beam Power in TEM_{00}	> 6 W	
	Beam Power in Higher Order Modes	$< 4 \times 10^{-5}$ W	

3.3. ISC

3.3.1. Optical

3.3.1.1 Diagnostic Sensing Beams

The IOO delivers diagnostic beams to the ISC subsystems from Faraday Isolators located in WHAM 1 (WA 4 km IFO), in WHAM 7 (WA 2 km IFO), and LHAM 11 (LA 4 km IFO) through HAM viewports. These beams will have spot sizes of 2 mm ±0.1 mm with nominal powers of 300 mW and up to 6 W during lock acquisition of the IFO.

Table 6: IOO/ISC Optical Interfaces for the 2 km IFO

Optical Interface	*Interface Description*	*Value/Tolerance*
COC Length/ Alignment Sensing Beam	Location of Handoff of back-reflected diagnostic beam from COC through IOO to ISC subsystem	Viewport WH7A1F4
	Beam Size at Interface	1.82 mm $\pm 0.1 mm$
	Beam Divergence Half Angle	0.186 mrad (converging)
	Incident Angle on Viewport	5°
	Beam Power	0.5 W
	Polarization	S pol.

Table 7: IOO/ISC Optical Interfaces for the 4 km IFO

Optical Interface	*Interface Description*	*Value/Tolerance*
COC Length/ Alignment Sensing Beam	Location of Handoff of back-reflected diagnostic beam from COC through IOO to ISC subsystem	Viewport WH1A1F4
	Beam Size at Interface	0.165 mm $\pm 0.1 mm$
	Beam Divergence Half Angle	0.208 mrad (diverging)
	Incident Angle on Viewport	5°
	Beam Power	0.5 W
	Polarization	S pol.

3.3.1.2 Optical Levers

The ISC provides optical levering for the mode matching telescope mirror MMT3 in the 2,4 km IFOs. The transmitter/receivers for the MMT3 optical lever is located on HAMs viewports (see Section 4.2.)

The optical lever beam contacts the MMT3 mirrors in the location **TBD/ASC.**

3.3.2. Mechanical

The IOO MC length and alignment systems are located on tables IOT1,7 which are owned by the ISC.

3.4. SEI

3.4.1. Mechanical

The in-vacuum IOO components are located on the seismic isolation stacks located in WHAM 1,2,7,8 and LHAM 11,12.

3.5. VACUUM

3.5.1. Mechanical

Viewports for bringing the main beam into the vacuum system and taking diagnostic beams out of the vacuum system to their respective diagnostic functions are located on the HAM covers. The locations are given in Table 8.

Table 8: Locations of IOO Viewports

Viewport	*Location*
2 km Main Beam Vacuum Feed-in	WH7B2F3
2 km PSL Intensity Stabilization Feed-out	WH7A2F5
2 km MC Diagnostic Beam Feed-out	WH7A2F3
4 km Main Beam Vacuum Feed-in	WH1B2F3
4 km PSL Intensity Stabilization Feed-out	WH1A2F5
4 km MC Diagnostic Beam Feed-out	WH1A2F3

A beam tube which encloses the main beam feed-in from the PSL/IOO table to the vacuum system is attached to the WHAM 1,7 HAM Viewports WH7B2F3, WH1B2F3.

3.6. CDS

3.6.1. Mechanical

Sensor/actuator heads (SAH's) for the Small Optics Suspensions are supplied by the CDS group. IOO will mount these in the suspensions as part of the suspension assembly and balancing during the installation process.

3.6.2. Electrical

The RF modulation signals for the resonant, non-resonant, and mode cleaner PDH sidebands are supplied to the IOO EOMs from CDS. The signal characteristics are given in Table 9.

Table 9: RF Signals into IOO

Sideband	*Frequency* (MHz)	*Modulation Depth* Γ	*Voltage, (pk-pk)*	*RF Power, RMS (into 50* Ω)
4 km IFO resonant, typ " max	24.493	0.47 1	4.7 V 10 V	55 mW 0.25 W
4 km IFO non-resonant	61.232 (**TBD ASC**)	0.055	0.6 V	~1 mW
4 km MC	33.289	0.1	1 V	2.5 mW
2 km IFO resonant, typ " max	29.486	0.47 1	4.7 V 10 V	55 mW 0.25 W
2 km IFO non-resonant	68.800 (**TBD ASC**)	0.055	0.6 V pk-pk	~1 mW
4 km MC	26.717	0.1	1 V	2.5 mW

Note: Modulation indices Γ are nominal; the modulation depths for the resonant sidebands are to range from 0-1. The range of modulation depth for the non-resonant sideband of **TBD ISC** will be provided by ISC.

3.6.2.1 EMI Control

The maximum RF power in the Pockel's cells in LIGO are less than 1/4 W and it will generate radiation field of about 0.5 V/m at a distance of 5 meters away from the source if that power is totally radiated (impedance matched to an antenna). The Pockel's cell to be used has a metal box housing which has two openings of 2 mm in diameter while the wavelength of the RF modulation filed to be used is at least 5 meters. The radiation from the opening will be negligibly small. However, the cables for the RF power need to be grounded at both ends and run as close to the grounding surface as possible.

3.6.3. PSL Table Mirror Actuators

ISC provides mode-cleaner length and alignment control signals to the PI-E-503 3-channel amplifier module located in CDS IOO racks **TBD/CDS**. CDS in turn provides signals to the PI S-330.30 two-axis tilting mirror actuators on the IOO/PSL table and the periscope.

3.6.4. Small Optics Suspensions

CDS takes input signals from the IOO for controlling small optics suspensions and delivers control signals to the suspensions. Table 10 displays the SOS interfaces to CDS.

Table 10: CDS SOS Interfaces

IFO	*Suspension*	*CDS Input from IOO*	*CDS Output to SOS*
2 km	MCM1	MC WFS Input Signal	SAH Control Signals
2 km	MCM2	MC RFPD	SAH Actuator Control Signals
2 km	MCM3	MC WFS Input Signal	SAH Actuator Control Signals
2 km	SM1	DC Input Control Signal	SAH Actuator Control Signals
2 km	SM2	DC Input Control Signal	SAH Control Signals
2 km	MMT1	DC Input Control Signal	SAH Actuator Control Signals
2 km	MMT2	DC Input Control Signal; AC 0.1 Hz 100 μm Dither	SAH Actuator Control Signals
4 km	MCM1	MC WFS Input Signal	SAH Actuator Control Signals
4 km	MCM2	MC RFPD	SAH Control Signals
4 km	MCM3	MC WFS Input Signal	SAH Actuator Control Signals
4 km	SM1	DC Input Control Signal	SAH Actuator Control Signals
4 km	MMT1	DC Input Control Signal	SAH Actuator Control Signals
4 km	MMT2	DC Input Control Signal; AC 0.1 Hz 100 μm Dither	SAH Actuator Control Signals

4 IOO LAYOUT

4.1. PSL/IOO Table

The PSL table contains the following IOO components:

- Phase modulators for the application of RF sidebands
- Lenses for mode matching into the MC
- A periscope for the stepping the beam up to the HAM viewport.
- Beam tubes to minimize air current and acoustic perturbations

4.1.1. Optical (ASAP)

The PSL/IOO table was modeled using ASAP to check effects of clipping, beam splitting, and out of plane elevation pointing stability. The MMT for the MC was also numerically analyzed for wavefront distortion from spherical aberration. The main results are

- beam clipping at 10 ppm occurs in the EOM aperture
- wave front distortions (higher order TEM modes) are limited to 10^{-2} in amplitude on the PSL table.

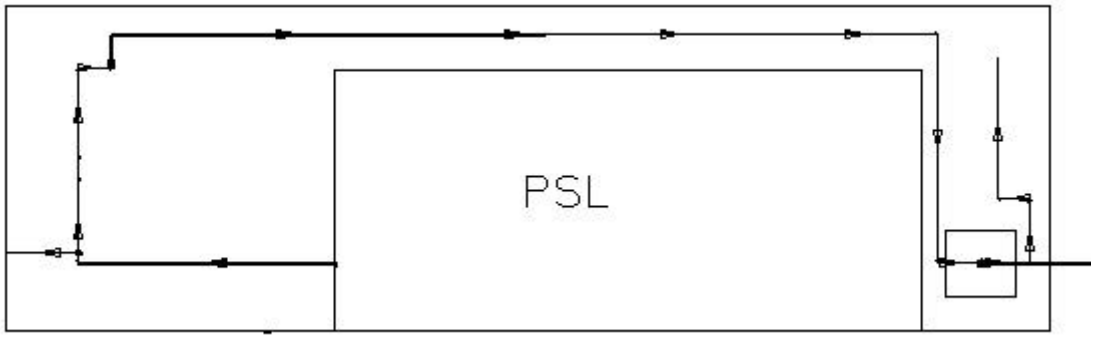

4.1.2. Mechanical

The mechanical layout for the 2 km PSL table showing complete optical and opto-mechanical mounting is shown in Figure 4.

Figure 4: 2 km PSL ACAD Opto-mechanical Layout

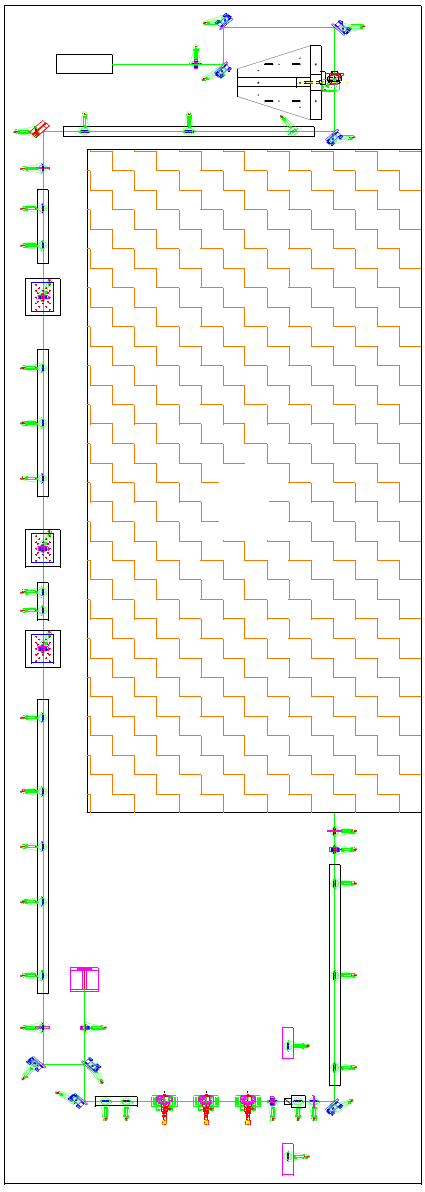

4.1.2.1 Periscope

4.1.2.1.1 Mechanical Design

Since the relative laser beam heights at the IOO/PSL table and at the input port of HAM1 has a 832 mm rise, a periscope is designed to raise the beam without change of the polarization of the light. The structure of the periscope has to maintain the stability of the supporting table and the lowest resonances have to be high enough to avoid amplification of ground noise. A simple structure comprising two tapered aluminum beams is designed to provide necessary stiffness. Figure 5 shows the dimensions of the basic structure. The top of the optical table (RS 4000 Table from Newport is assumed) has a typical maximum relative motion value of $< 1.3 \times 10^{-10}$ m (see Newport catalog). Assuming the top mirror on the periscope has an maximum amplification of motion relative to the table top by 110 that results in an maximum relative motion value of 1.4×10^{-8} m for the top mirror at 200 Hz, the output beam direction disturbance caused by this motion is about 3×10^{-8} rad which is negligibly small compared to the laser beam pointing angle fluctuations (in the order of μrad).

Figure 5: Basic structure of the periscope. Material: aluminum.

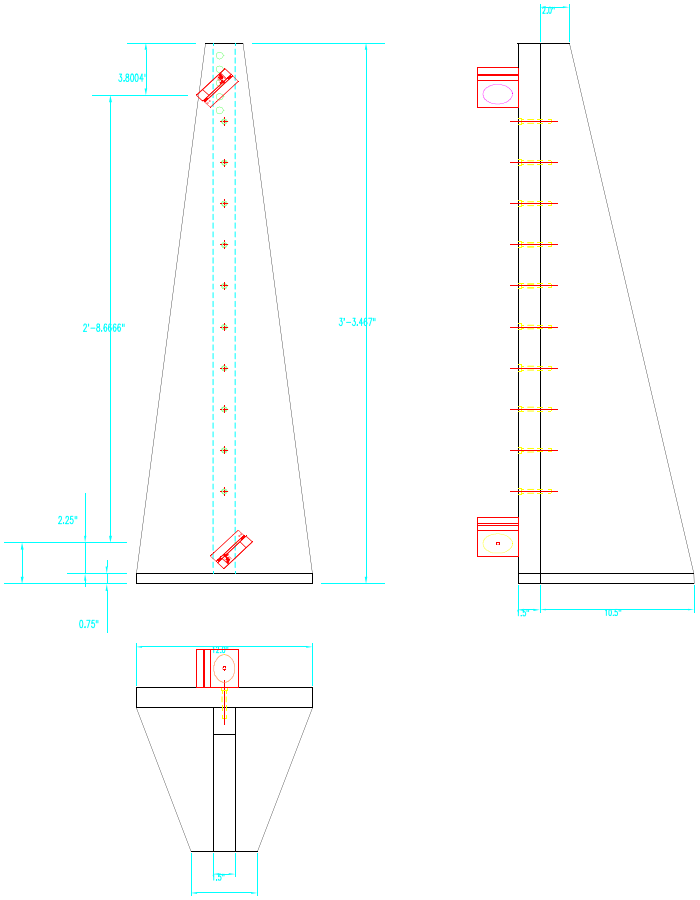

4.1.2.1.2 Resonances/Transfer Functions

Mike Fine calculated the lowest 6 resonance frequencies using finite element analysis, which are shown in Table 11. The transfer function of the periscope structure has not been calculated; however since the lowest frequency is above 200 Hz, the transfer function below 100 Hz can be safely assumed to be unity. Figure 6 shows the transfer functions calculated by Mike Fine at Caltech

Table 11: Calculated resonance frequencies of the periscope basic structure.

Mode No.	Resonance Frequencies (Hz)
1	203
2	301
3	317
4	659
5	748
6	820

using finite element modeling of the basic structure of the periscope. x direction is in the horizontal plane and parallel to the optical mounting surface, y is the horizontal plane and perpendicular to x, ann z is the vertical direction.

Figure 6: Finite element modeling of the transfer functions of the periscope basic structure.

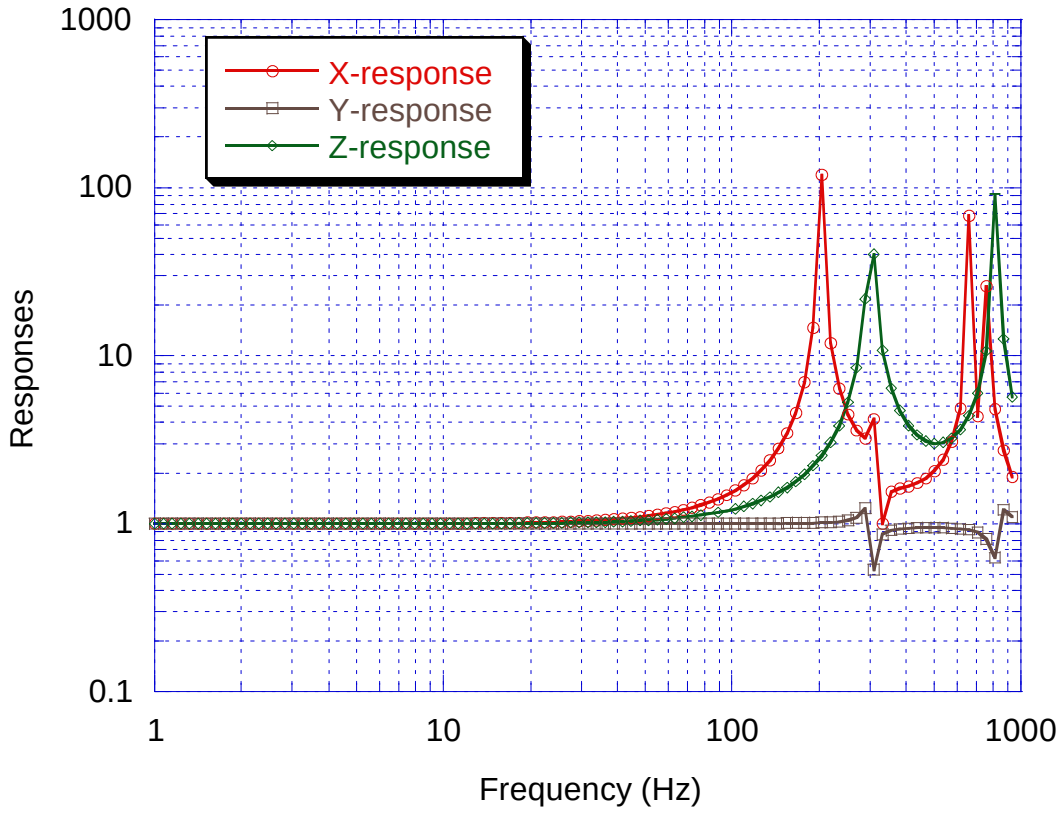

4.1.2.2 Beam Tube into HAMs

The periscope fits under the planned table cover. A hole is required in the cover for the exit beam, with either a nozzle (3-4 inch diameter TBD/PSL) or holes for a flange attachment. A tube will protect the beam between the cover and the HAM viewport.

4.2. In Vacuum Layouts

Complete in-vacuum layouts are for the 2 km and 4 km IOO subsystems are shown below.

4.2.1. 4 km IFO (HAM 1,2)

4.2.1.1 Mechanical (AutoCAD) Design

Figure 7: HAM1,2 Layout

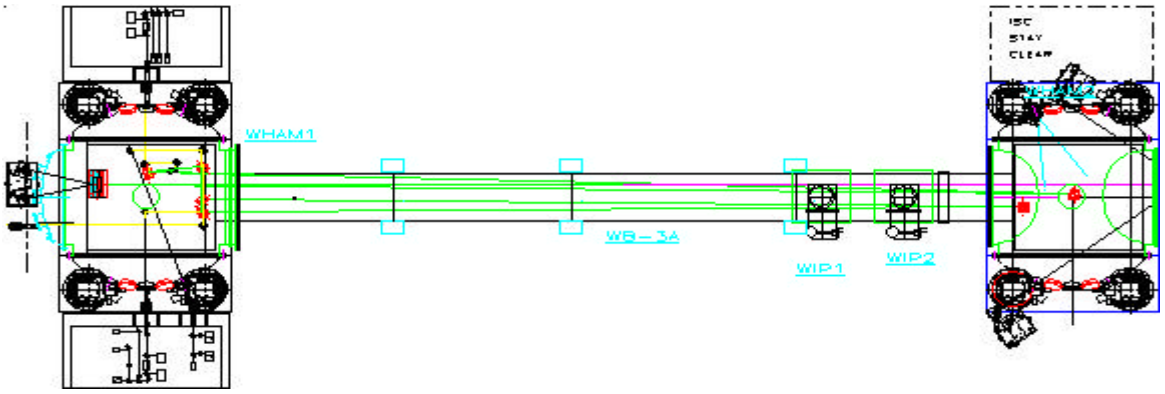

Figure 8: HAM 1 Detailed Layout

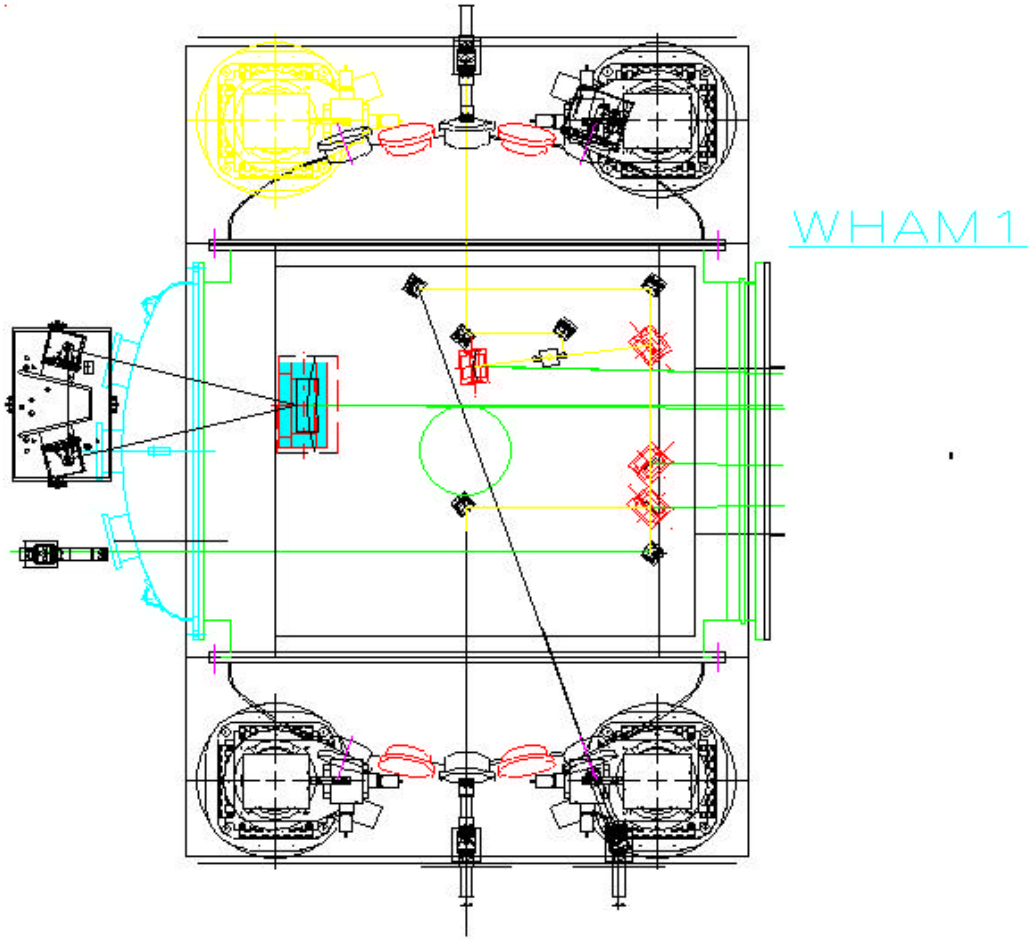

Figure 9: HAM2 Detailed Layout

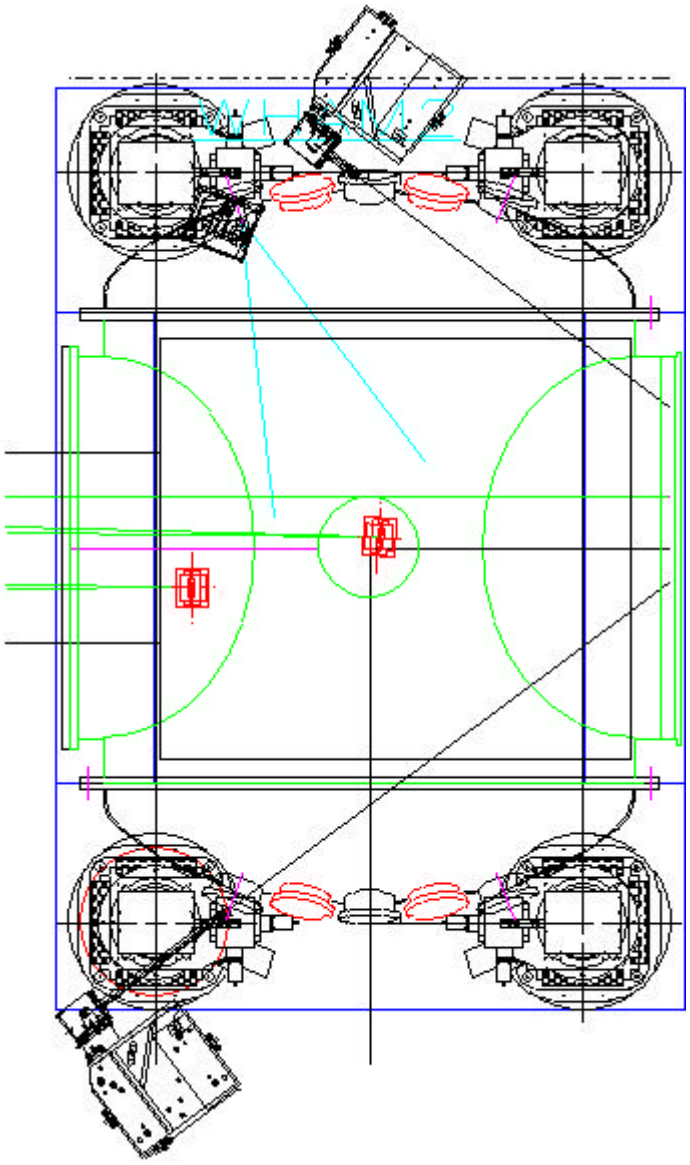

4.2.1.1.1 Baffles

The baffles located in HAM2 separating the IOO from the COC are provided by COS. Using analysis by COS, we have concluded that beam dumps for the beams which reflect off the vacuum feedthrough ports are not necessary. Should experimental findings or changes in the design dictate the necessity of beam dumps, space on the stacks has been provided.

4.2.1.2 Optical (ASAP) Design

Figure 10: ASAP Optical Layouts (Plan and Elevation) of HAM1

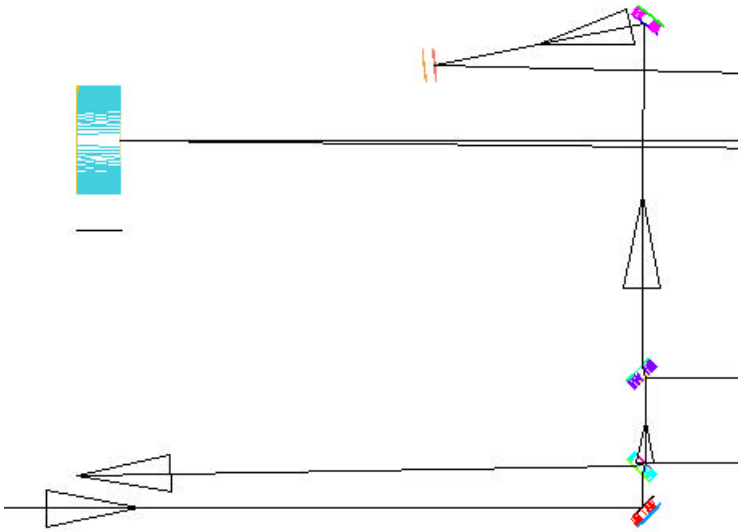

Plan View

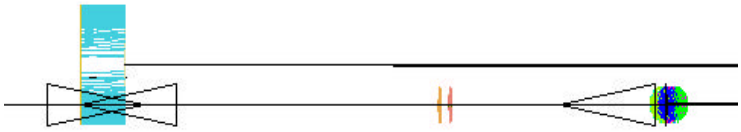

Elevation View

Figure 11: ASAP Optical Layouts (Plan and Elevation) of HAM2

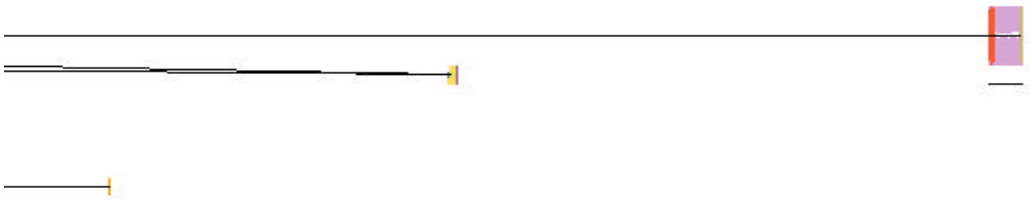

Plan View

Elevation View

4.2.2. 2 km IFO (HAM 7,8)

4.2.2.1 Mechanical (AutoCAD) Design

Figure 12: HAM7,8 Layout

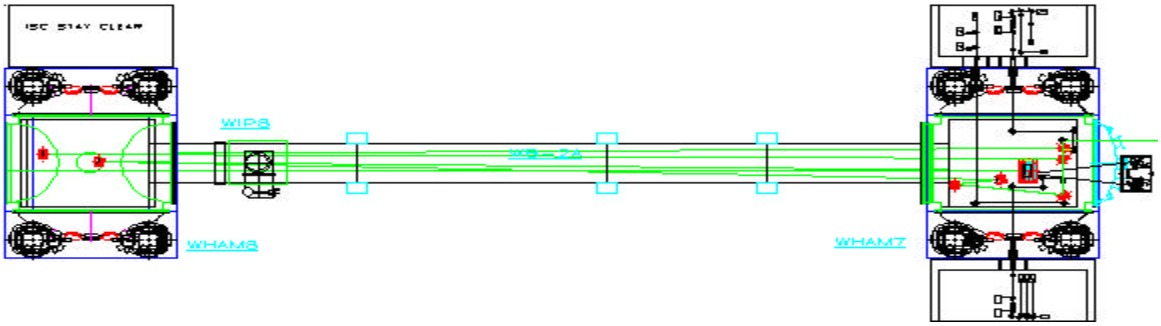

Figure 13: HAM7 Detailed Layout

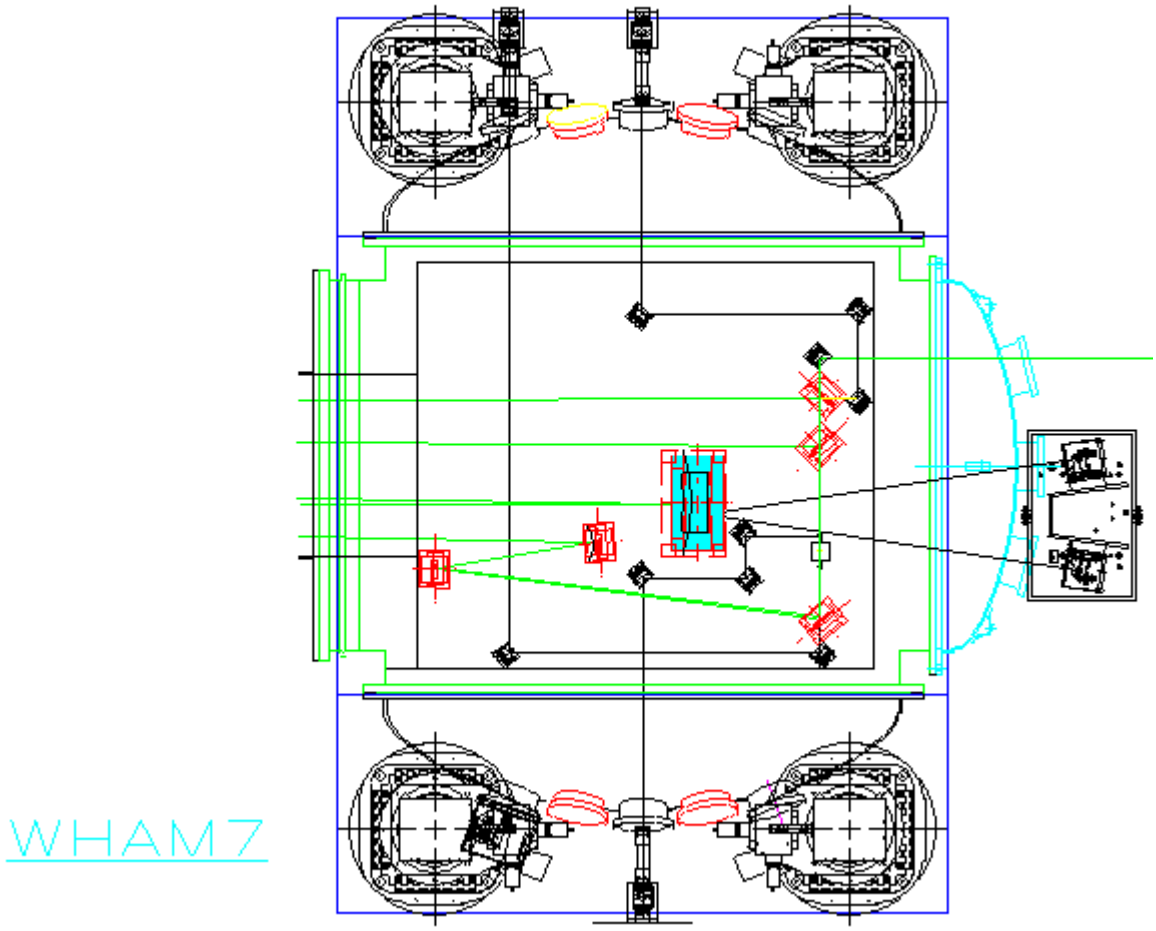

Figure 14: HAM8 Detailed Layout

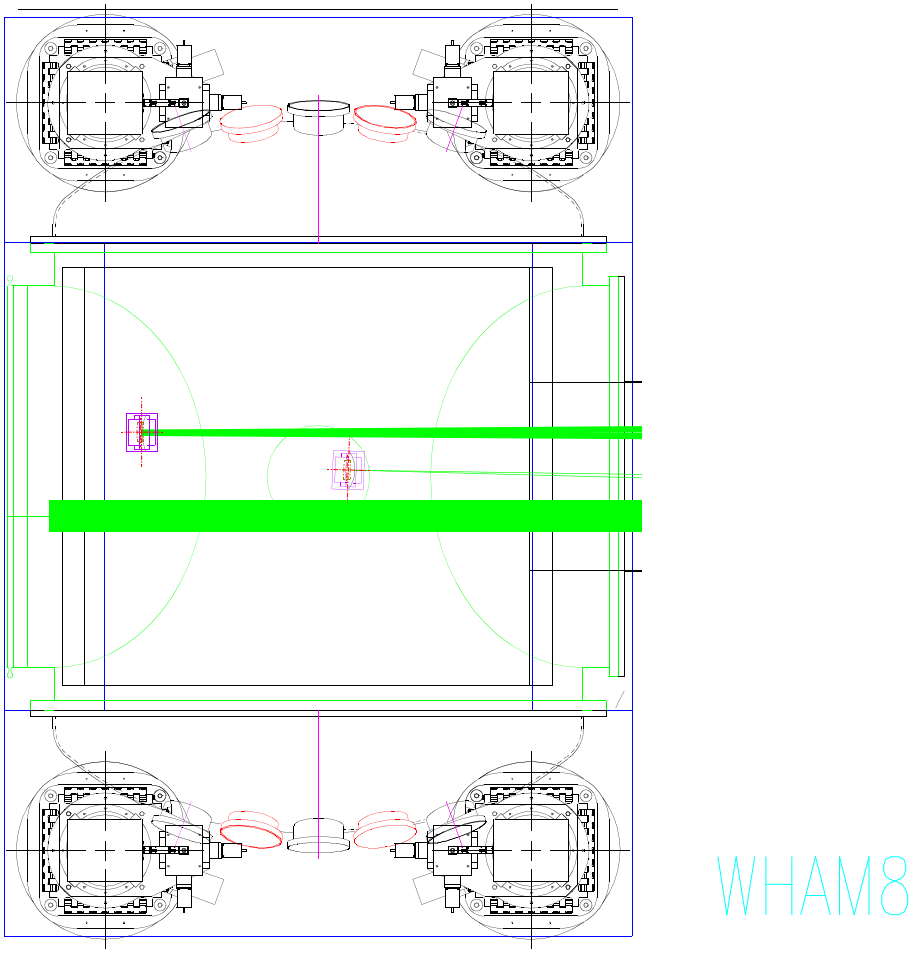

4.2.2.1.1 Baffles

The baffles located in HAM2 separating the IOO from the COC are provided by COS. Using analysis by COS, we have concluded that beam dumps for the beams which reflect off the vacuum feedthrough ports are not necessary. Should experimental findings or changes in the design dictate the necessity of beam dumps, space on the stacks has been provided.

4.2.2.2 Optical (ASAP) Design

Figure 15: ASAP Optical Layouts (Plan and Elevation) of HAM7

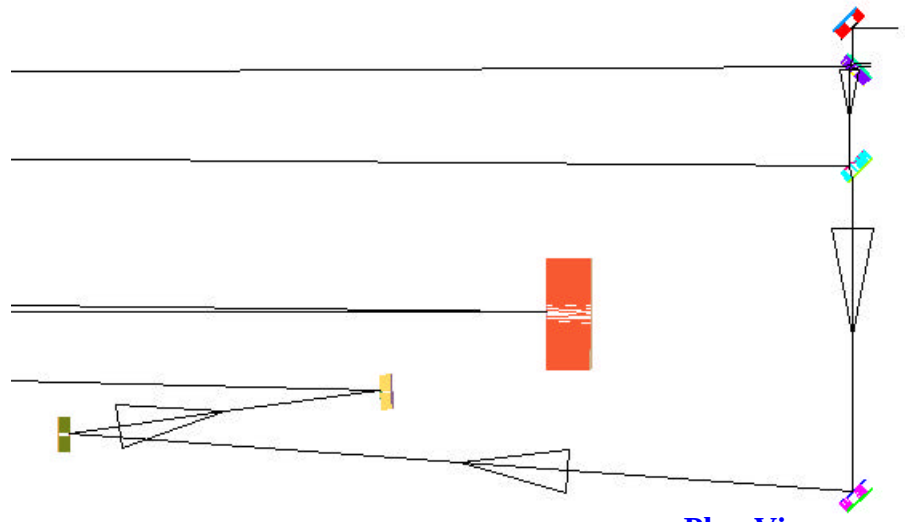

Plan View

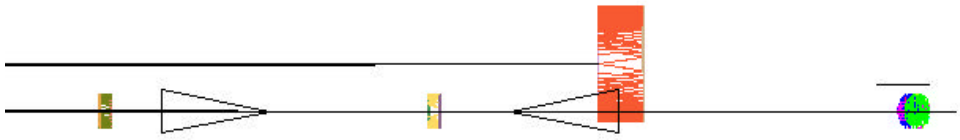

Elevation View

Figure 16: ASAP Optical Layouts (Plan and Elevation) of HAM8

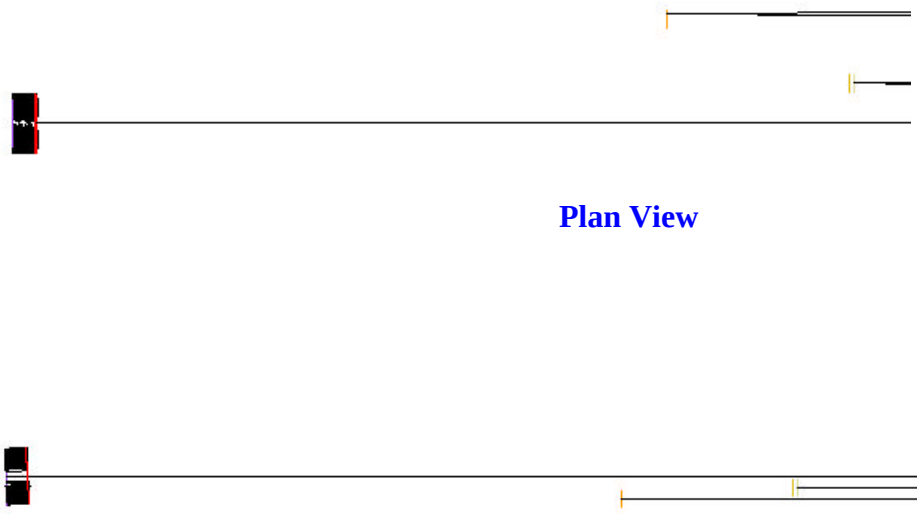

Plan View

Elevation View

4.3. IOO LSC/ASC Tables

The IOT and ISC tables provide length and alignment sensing for the MC and the IFO.

The IOT tables contain:

- MC length sensing RF photodiode and associated optics and mounts
- MC WFS diodes and associated optics and mounts
- PSL intensity stabilization RF photodiode and associated optics and mounts
- MC noise and RFAM monitoring RF photodiode and associated optics and mounts
- Optical spectrum analyzer for RF sideband monitoring after the MC

Space is also reserved on the IOT tables for MC mode-matching measurement using bullseye sensors.

The ISC tables contain:

- IFO length sensing RF photodiode and associated optics and mounts
- IFO WFS diodes and associated optics and mounts
- IFO mode matching ‘bullseye’ RF photodiode and associated optics and mounts

4.3.1. IOT1

Figure 17: IOT1 Table Layout

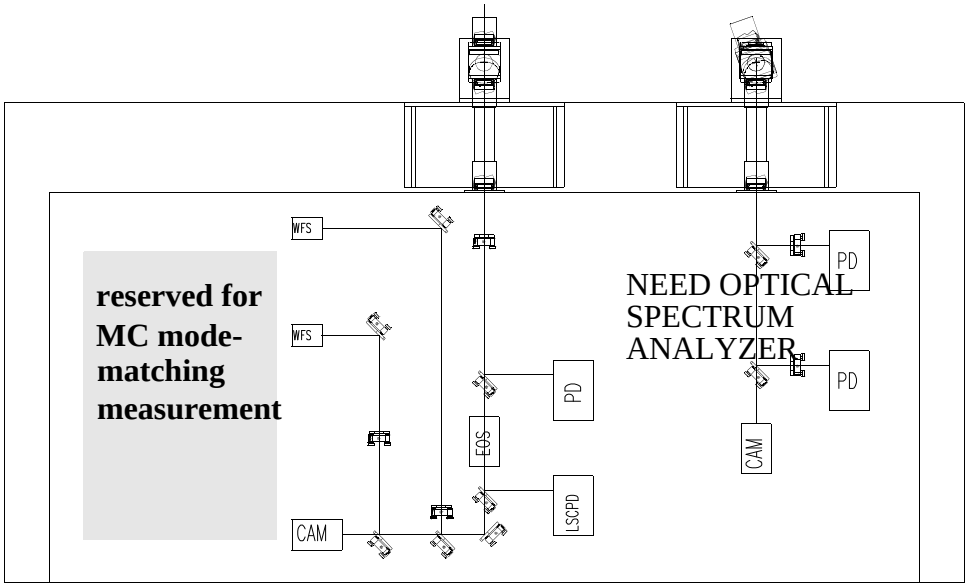

4.3.2. IOT7

Figure 18: IOT7 Table Layout

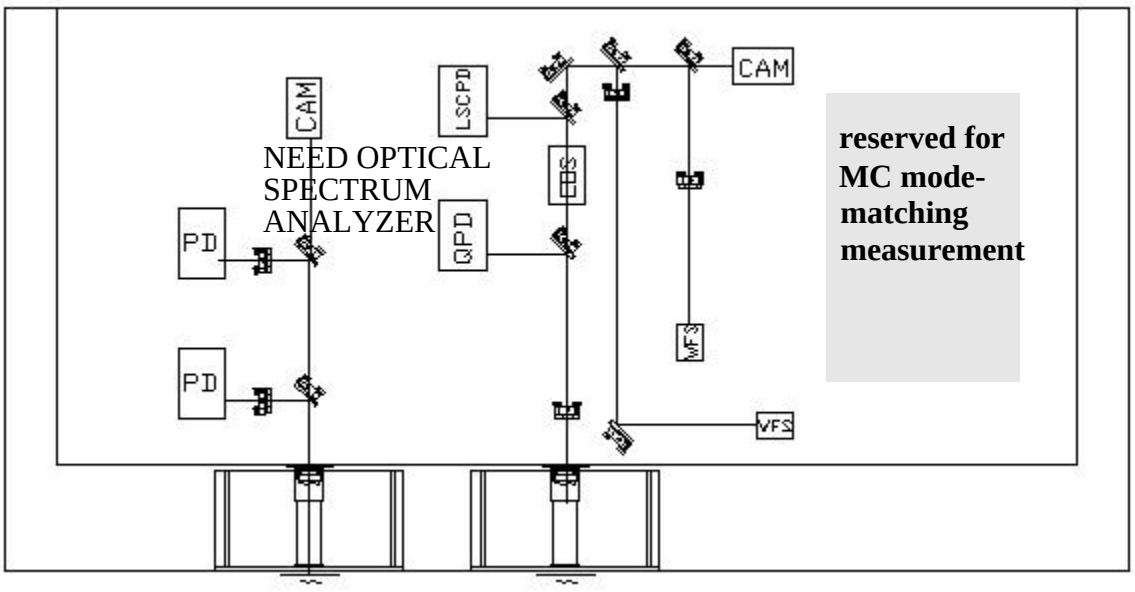

4.3.3. ISC1

Figure 19: ISC1 Table Layout

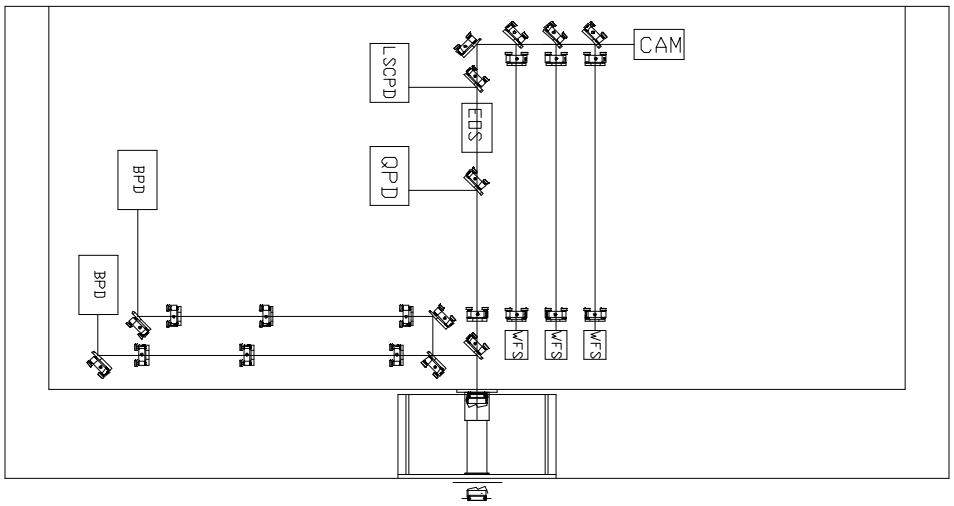

4.3.4. ISC7

Figure 20: ISC7 Table Layout

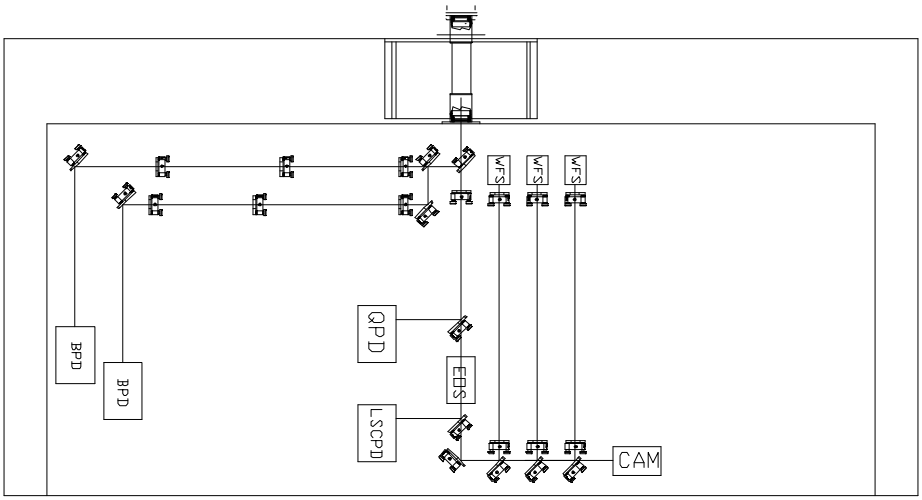

5 RF MODULATION SYSTEM

5.1. Design

The IOO RF modulation system must provide both the resonant and nonresonant sidebands required by the ISC subsystem. It also must provide an RF sideband for the mode cleaner length control. Three Pockels cells provide phase modulation of the carrier from the PSL.

The LIGO core optics require two modulation frequencies:

1. The first modulation frequency gives upper and lower sidebands that are resonant in the recycling cavity but not resonant in the interferometer arm cavities. These are used for controlling the lengths of the interferometer and for aligning the arm cavities and the beam splitter.

2. The second modulation frequency gives upper and lower sidebands that are not resonant in the recycling cavity. These are used for alignment of the recycling mirror.

The values of these frequencies are set by the lengths of the respective cavities. The resonant sideband frequency must satisfy

$$f_{res} = \left(k + \frac{1}{2}\right)\frac{c}{2L_{rc}}$$

where k = 0,1,2... and L_{rc} is the recycling cavity length. The extra factor of 1/2 occurs because the carrier is resonant in the arm cavities whereas the sidebands are not resonant in the arms, giving a extra 180^{o} phase shift in the reflectivity of the arms.

The nonresonant sideband frequency is chosen to miss the recycling cavity resonances. Both the resonant and nonresonant sidebands must be equal to one of the mode cleaner resonances, because the RF modulation is imposed before the mode cleaner. The resonant frequencies of the mode cleaner are:

$$f_{mc} = n\frac{c}{2L_{mc}}$$

where n is an integer (1,2,3...) and L_{mc} the mode cleaner length.

5.2. Constraints

The mode cleaner and recycling cavities span vacuum chambers whose separations determine the cavity lengths. There is some flexibility on account of the size of the optical tables in these chambers.[1] The mode cleaner for the 4-km interferometer occupies HAM-1 and HAM-2; the recycling mirror is in HAM-3; the input test masses are in BSC-1 and BSC-3. The mode cleaner for the 2-km interferometer occupies HAM-7 and HAM-8; the recycling mirror is in HAM-9; the input test masses are in BSC-7 and BSC-8.

1. For details see M. Zucker and P. Fritschel, LIGO-T960122-00-I, D. Coyne, LIGO-T970068-00-D, D.B. Tanner, LIGO-T-970xxx-03-D.

In addition to the separations of the vacuum chambers, a number of factors affect the optical lengths of the mode cleaner and recycling cavities. These include the footprints of the suspensions, mirror thicknesses, the triangular path of the mode cleaner, substrate refractive index, the space required for other optical components, the offset of the optical centerline from the centerlines of the beam tubes, and the Schnupp asymmetry of the core optics. In addition, the modulation frequencies must miss all the harmonics of the arm free spectral range: 37.5 kHz in the 4-km interferometer; 75 kHz in the 2-km interferometer.

5.3. Resonant sidebands.

5.3.1. Resonant sideband frequency.

The RF frequencies for the resonant sidebands have been chosen according to the following criteria:

- The frequency must be consistent with the resonant cavity lengths described previously.
- The lengths of the two cavities (mode cleaner and recycling) shall not be an integer multiple of each other (so that harmonics of the nonresonant sideband do not resonate in the recycling cavity).
- The frequency shall be as low as possible.

The frequencies and lengths for the two interferometers are in Table 12:

Table 12: Modulation frequencies for resonant sidebands and corresponding optical lengths.

IFO	n,k	f_{res} (MHz)	L_{mc} (mm)	L_{rc} (mm)
4-km	2,1	24.493	12240	9188
2-km	3,2	29.486	15251	12715

See the documents in footnote 1 for calculations justifying these frequencies.

5.3.2. Resonant sideband modulation index.

The modulation index for the resonant sidebands is specified in the SYS document as $\Gamma = 0.47$. The modulation index is to be adjustable over a range of $0< \Gamma<1$ (**TBD/ISC**).

With a nominal 6 W delivered to the core optics, a modulation index of $\Gamma= 0.47$ will provide 5.36 W in the carrier and 310 mW in each first-order sideband. A modulation index of $\Gamma = 1$ will provide 3.51 W in the carrier and 1.16 W in each first-order sideband.

5.3.3. Pockels cell

Phase modulation in a Pockels cell is achieved by electrically varying the optical path length of the light through an electro-optic crystal. The crystal must be aligned with the light polarization in order to avoid residual amplitude modulation to within 0.17^{o}. By using a resonant device, the RF drive voltages can be kept low. In this configuration, the 50Ω output of the RF amplifier is

matched to the capacitive load of the crystal by a resonant circuit. Typical RF bandwidth is 1%, which is larger than the tuning range of the RF generators.

A suitable modulator is MgO:LiNbO3 (New Focus 4003) which has a phase shift of 0.2 rad/Volt. Thus, 4.7 V peak-to-peak is necessary for $\Gamma = 0.47$ and 10 V peak-to-peak for $\Gamma = 1$. The latter voltage implies a power load of 1/4 W RMS from the RF system.

5.4. Nonresonant sidebands.

5.4.1. Nonresonant sideband frequency.

The RF frequencies for the nonresonant sidebands have been chosen according to the following criteria:

- The frequency must be consistent with the mode cleaner cavity lengths described above.
- The frequency shall be sufficiently high that the effect of first-order mixing of the resonant and non resonant sidebands is reduced.
- The frequency shall not be an integer multiple of the resonant sideband frequency.
- The frequency shall be within the demonstrated range of the RF photodiodes (70 MHz TBD-ASC).

The frequencies for the two interferometers are in Table 13.

Table 13: Modulation frequencies for nonresonant sidebands.

IFO	n	f_{nr} (MHz)
4-km	5	61.232
2-km	7	68.800

5.4.2. Nonresonant sideband modulation index.

The modulation index for the nonresonant sidebands has a nominal value of $\Gamma = 0.055$. With a nominal 6 W delivered to the core optics, a modulation index of $\Gamma = 0.055$ will provide 4 mW in each first-order sideband.

5.4.3. Pockels cell

The Pockels cell for the non resonant sidebands will be identical to the one used for the resonant sidebands (New Focus model 4003). The voltage for $\Gamma = 0.055$ is 0.6 V peak-to-peak, making the RF power required 0.9 mW RMS. The Pockels cell is capable of modulation indices up to $\Gamma = 1$ if 1/4 W RMS RF power is supplied.

5.5. Modulation for mode cleaner length control.

5.5.1. Mode-cleaner modulation frequency.

We.choose frequencies which have all harmonics nonresonant in the mode cleaner, and which have mixing sidebands with both resonant and nonresonant sidebands which are nonresonant in the mode cleaner.

Table 14: Modulation frequencies for mode cleaner locking.

IFO	f_{lock} (MHz)
4-km	33.289
2-km	26.717

5.5.2. Mode cleaner modulation index.

The modulation index for the mode-cleaner sidebands is $\Gamma = 0.1$.[1] With a nominal 6 W from the PSL, a modulation index of $\Gamma = 0.1$ will provide 13 mW in each first-order sideband.

5.5.3. Pockels cell performance

The Pockels cell for the mode-cleaner sidebands will be identical to the one used for the other sidebands (New Focus 4003). The voltage for $\Gamma = 0.1$ is 1 V peak-to-peak, making the RF power required 2.5 mW. The Pockels cell is capable of modulation indices up to $\Gamma = 1$ if 1/4 W RF power is supplied.

5.6. Modulation cross products.

The output of the RF modulation section will be phase-modulated light, of the form

$$E = e^{-i\omega t + i\Gamma_1 \cos(\Omega_1 t) + i\Gamma_2 \cos(\Omega_2 t) + i\Gamma_3 \cos(\Omega_3 t)}$$

where ω is the infrared frequency of the carrier, Γ is the modulation index and Ω_i is the frequency of the i^{th} sideband. This formula can be expanded using

$$e^{i\Gamma\cos(\Omega t)} = J_0(\Gamma) + 2i\sum_{k=1}^{\infty}(-1)^{k-1}J_{2k-1}(\Gamma)\cos[(2k-1)\Omega t]$$

$$-2\sum_{k=1}^{\infty}(-1)^{k-1}J_{2k}(\Gamma)\cos[2k\Omega t]$$

1. Mode Cleaner Length/Frequency Control Design, P. Fritschel, N. Mavalvala, D. Ouimette, LIGO-T970218-01-D

When this is written out, one sees that with more than one modulation frequency, there will be output at sums and differences of each frequency.

5.6.1. Modulation cross products from mode-cleaner sidebands.

All modulation cross products involving the mode cleaner locking sideband (Ω_3) will be non-resonant in the mode cleaner and will be attenuated (in power) by a factor of 10^6.

5.6.2. Modulation cross products from resonant and non-resonant sidebands.

All sidebands and mixing products from the resonant sideband ($\Omega_{1)}$ and the non-resonant sideband (Ω_2) pass through the mode cleaner. The frequencies and amplitudes of these "sidebands on sidebands" are given in Table 15.[1] We have listed all intermodulation products above 10^{-9} in amplitude for frequencies up to the non-resonant sideband Ω_2, and all products above 10^{-7} up to 2.5 times this frequency. (For simplicity we take 25 and 62.5 MHz as the 4-km interferometer modulation frequencies; 30 and 80 MHz as the 2-km frequencies. The input light has unit amplitude.) We have also listed whether the products are in phase or in quadrature with the carrier and whether the new frequency will be admitted by the recycling cavity or not.

Table 15: RF sideband frequencies.

Product	*Phase*	*4-km*		*2-km*		*Amplitude*
		MHz	RC admit	MHz	RC admit	
Carrier	Re	0	Y	0	Y	0.945
$5\Omega_1 - 2\Omega_2$	Im	0	Y	10	N	2.24×10^{-9}
$\Omega_2 - 2\Omega_1$	Im	12.5	N	20	N	7.45×10^{-4}
$3\Omega_1 - \Omega_2$	Re	12.5	N	10	N	5.86×10^{-5}
Ω_1	Im	25	Y	30	Y	0.228
$2\Omega_2 - 4\Omega_1$	Re	25	Y	40	N	4.75×10^{-8}
$\Omega_2 - \Omega_1$	Re	37.5	N	50	N	0.00628
$4\Omega_1 - \Omega_2$	Im	37.5	N	40	N	3.45×10^{-6}
$2\Omega_1$	Re	50	N	60	N	0.0271
$2\Omega_2 - 3\Omega_1$	Im	50	N	70	N	8.06×10^{-7}
Ω_2	Im	62.5	N	80	N	0.0256
$5\Omega_1 - \Omega_2$	Re	62.6	N	70	N	1.62×10^{-7}
$3\Omega_1$	Im	75	Y	90	Y	0.00213
$2\Omega_2 - 2\Omega_1$	Re	75	Y	100	N	1.02×10^{-5}

1. *Impact of Non-resonant Sidebands on Length Sensing Signals*, J. Camp, LIGO-T970097-00-D

Table 15: RF sideband frequencies.

Product	*Phase*	*4-km*		*2-km*		*Amplitude*
		MHz	RC admit	MHz	RC admit	
$\Omega_1 + \Omega_2$	Re	87.5	N	110	N	0.00628
$4\Omega_1$	Re	100	N	120	N	1.25×10^{-4}
$2\Omega_2 - \Omega_1$	Im	100	N	130	N	8.64×10^{-5}
$2\Omega_1 + \Omega_2$	Im	112.5	N	140	N	7.45×10^{-4}
$2\Omega_2$	Re	125	N	160	N	3.57×10^{-4}
$5\Omega_1$	Im	125	N	150	Y	5.91×10^{-6}
$3\Omega_1 + \Omega_2$	Re	137.5	N	170	N	5.86×10^{-5}
$\Omega_1 + 2\Omega_2$	Im	150	N	190	N	8.64×10^{-5}

5.6.3. Modulation cross product power at the GW demodulation frequency.

RF photodiodes produce signals proportional to the light intensity or field squared. (The intensity, in turn, depends on the highly dispersive behavior of the interferometer.) The critical frequency is Ω_1, 25 MHz in the case of the 4-km interferometer. The other key factor is whether the *E*-field is admitted by the recycling cavity. Most of the intemodulation products are not admitted into the recycling cavity, so their amplitude at the dark port is reduced by the transmission of the recycling mirror. The contributions to the RF power at 25 MHz (which is incident towards the beam splitter, assuming 6 W in the carrier) are given in Table 16.

Table 16: Power at 25 MHz in 4-km instrument.

Mixing of	*Admitted to RC*	*Power (W)*
$(2\Omega_2 - \Omega_1) - 3\Omega_1$	$3\Omega_1$	9.25×10^{-8}
$(2\Omega_2 - 3\Omega_1) - \Omega_1$	Ω_1	9.25×10^{-8}
$(\Omega_2 - 2\Omega_1)^2$	No	4.68×10^{-8}
$(\Omega_2 - \Omega_1) - (3\Omega_1 - \Omega_2)$	Neither	3.11×10^{-8}
$2\Omega_2 - 4\Omega_1$	Neither	1.13×10^{-8}
$\Omega_2 - (4\Omega_1 - \Omega_2)$	Neither	7.53×10^{-9}
$(3\Omega_1 - \Omega_2) + (\Omega_2 - 2\Omega_1)$	Neither	3.67×10^{-9}

By comparison, shot noise on 6 W is 1.06×10^{-9} W/rHz. The worst cases are $(2\Omega_2 - \Omega_1) - 3\Omega_1$ and $(2\Omega_2 - 3\Omega_1) - 1\Omega_1$. These essentially are the same product, and are about 10x the 100 Hz shot noise level.

6 MODE CLEANER

The mode cleaner serves several purposes in LIGO. It filters the non TEM_{00} components of the PSL output light, reduces amplitude and frequency noise of the light, contributes to frequency stability of the laser, decreases beam jitter (motion), and filters any incorrectly-polarized component introduced by the optics in front of it.

6.1. 4 km IFO MC

6.1.1. Optics / Tolerances

Table 17 lists the optical parameters of the 4 km mode cleaner.

Table 17: Optical parameters for the 4-K mode cleaners

Item	*Unit*	4K IFO	
Plane mirror transmittance		0.002	+/- 100ppm
Plane mirror reflectance		0.998	+/- 100ppm
Curved mirror transmittance		1E-05	+0, -10ppm
Rear surface AR coating		>99.8%	+0.2%,-0
Mirror absorbance/scattering	each	<0.00010	
Finesse		1550	
Free spectral range	MHz	12.246	
Cavity full width/half max	kHz	7.83	
Cavity full width/half max	nm	0.342	
Cavity optical half-length	mm	12240	
Curved mirror radius of curvature	mm	17250	+250,-350
g = 1 - L/R		0.290	
waist size	mm	1.629	
Raleigh range	m	7.83	
Beam divergence	μrad	208	
1 ppm intensity, curved mirror	mm	15.9	
100 ppm intensity, curved mirror	mm	13.0	

Detailed specifications of the 2 km, 4 km and 2 km MC mirror blanks can be found in LIGO-D970533,34,35. (incorrectly assigned D numbers)

Detailed CAD drawings for the mirror blanks can be found in LIGO-D970536,37,38

Detailed specifications for the substrates can be found in LIGO-E970146,44,43.

Detailed CAD drawings for the substrates can be found in LIGO-D970589,87,86

Table 18 lists the mirror dimensions for the 4 km mode cleaner. The mirror size is set by the use of Small Optical Suspensions (SOS) in the mode cleaner. The coating diameter on the curved mirror is smaller than the physical diameter to provide additional clipping of higher-order modes, which spill over the coated area.

Table 18: Physical parameters for the 4K mode cleaner

Item	*Unit*	4K IFO	
Mirror thickness (at max thickness)	mm	25	+0, -.5
Mirror wedge angle	mrad	8.73	+0.15, -0 mrad
Mirror diameter	mm	75	+1, -0
Curved mirror radius of curvature	mm	17250	+250,-350
Coating diameter (curved mirror)	mm	25	
Flat mirror radius of curvature	km	>80	
Coating diameter (flat mirrors)	mm	70	

6.1.2. Small Optics Suspensions for the 4-km mode cleaner.

The mode cleaners employ Small Optic Suspensions. These are described in *Small Optics Suspensions Final Design,* S. Kawamura, *LIGO-T970135-02-D.* The electronics that drive the suspensions are designed to the following requirements:

Table 19: SOS Parameters for the 4-km Mode Cleaner

Parameter	*Value*
Length Dynamic Range	27 μm pk-pk
Angular Dynamic Range	1.5 mrad pk-pk
Noise	3×10^{-18} m/rtHz

6.1.3. Length and Alignment Controls

ISC has the responsibility to design the length and alignment controls. IOO will deliver the beam PI actuators on the IOO table and on the periscope.

6.1.4. Mode Matching Optics

The mode matching onto the mode cleaner is done with a three refractive lens design. The constraints on the problem were that the lenses need to lie on the IO/PSL table, match the waist in the Pockels cells to the waist of the mode cleaner, use standard optics available through a vendor, and offer a wide range of adjustment. The parameters are given in Table 20.

Table 20: Mode matching into 4k MC

Parameter	*Value*
Waist size in center of second Pockels cell	0.0396 mm
Distance to MML_1 from waist in Pockels cell	248.23 cm
Distance from MML_1 to MML_2	41.55 cm
Distance from MML_2 to MML_3	103.91 cm
Distance from MML_3 to MC waist	749.42 cm
Waist size in MC	0.1629 cm
Nominal focal length of MML_1 (focal length for 1064 nm)	100 cm (114.56 cm)
Nominal focal length of MML_2 (focal length for 1064 nm)	-100 cm (-114.56 cm)
Nominal focal length of MML_3 (focal length for 1064 nm)	300 cm (343.62 cm)

The adjustablility of the telescope can be seen in Figure 21. This shows that the telescope can adjust for changes in waist position due to shifts in optical path length of more than 15 cm while holding the waist size constant. It can also adjust for changes in waist size in either the MC waist or the waist in the pockel cell of 10% easily. The spot size on all the lenses is about 2 mm, making the optic relatively slow, keeping aberrations to a minimum. A major advantage to this design is that we have made the lenses in both the 4k and the 2k machine the same without sacrificing flexibility.

Figure 21: Adjustment of Mode Matching into 4k MC

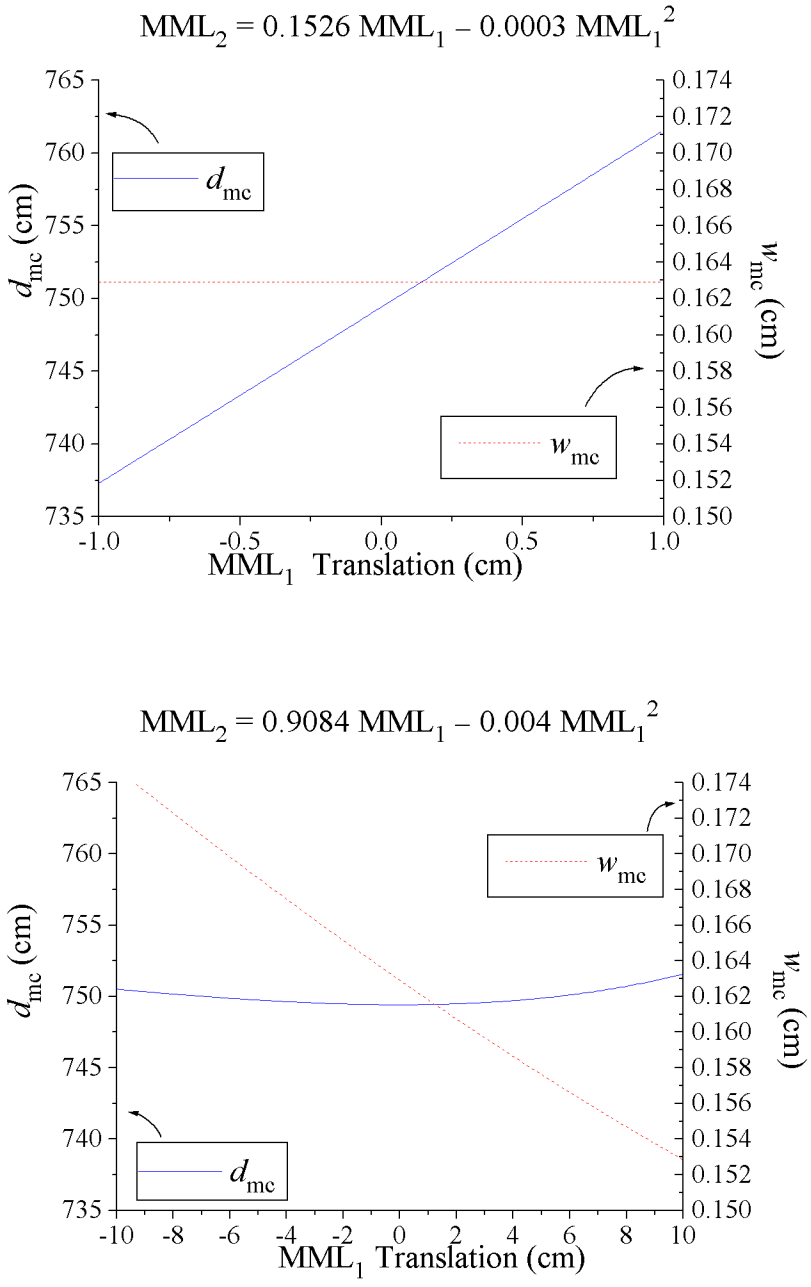

6.2. 2 km IFO MC

6.2.1. Optics

Table 21 lists the optical parameters chosen for the 2 km mode cleaner. The length *L* differs from the 4-km interferometers because of the differences in the separation of their HAM chambers. The

parameters for the 2-km interferometer are then an appropriately scaled version of those for the 4-km interferometer.

Table 21: Optical parameters for the 2K mode cleaner

Item	*Unit*	2K IFO	
Plane mirror transmittance		0.002	+/- 100ppm
Plane mirror reflectance		0.998	+/- 100ppm
Curved mirror transmittance		1E-05	+0, -10ppm
Rear surface AR coating		>99.8%	+0.2%,-0
Mirror absorbance/scattering	each	<0.00010	
Finesse		1550	
Free spectral range	MHz	9.829	
Cavity full width/half max	kHz	6.26	
Cavity full width/half max	nm	0.427	
Cavity optical half-length	mm	15251	
Curved mirror radius of curvature	mm	21500	+300, -400
g = 1 - L/R		0.291	
waist size	mm	1.818	
Raleigh range	m	9.76	
Beam divergence	μrad	186	
1 ppm intensity, curved mirror	mm	17.7	
100 ppm intensity, curved mirror	mm	14.5	

Table 22 lists the mirror dimensions for the 2 km mode cleaner. The mirror size is set by the use of Small Optical Suspensions (SOS) in the mode cleaner. The coating diameter on the curved mirror is smaller than the physical diameter to provide additional clipping of higher-order modes, which spill over the coated area.

Table 22: Physical parameters for the 2K mode cleaner

Item	*Unit*	2K IFO	
Mirror thickness	mm	25	+0, -.5
Mirror wedge angle	mrad	8.73	+0.15, -0 mrad
Mirror diameter	mm	75	+1, -0

Table 22: Physical parameters for the 2K mode cleaner

Item	*Unit*	2K IFO	
Curved mirror radius of curvature	mm	21500	+300, -400
Coating diameter (curved mirror)	mm	28	
Flat mirror radius of curvature	km	>80	
Coating diameter (flat mirrors)	mm	70	

6.2.2. Small Optics Suspensions for the 2-km Mode cleaner

The mode cleaners employ Small Optic Suspensions. These are described in *Small Optics Suspensions Final Design,* S. Kawamura, *LIGO-T970135-02-D.* The electronics that drive the suspensions are designed to the following requirements:

Table 23: SOS Parameters for the 2-km Mode Cleaner

Parameter	*Value*
Length Dynamic Range	27 μm pk-pk
Angular Dynamic Range	1.5 mrad pk-pk
Noise	3×10^{-18} m/rtHz

6.2.3. Length and Alignment Controls

ISC has the responsibility to design the length and alignment controls. IOO will deliver the beam PI actuators on the IOO table and on the periscope.

6.2.4. Mode Matching Optics

The mode matching onto the mode cleaner is done with a three refractive lens design. The constraints on the problem were that the lenses need to lie on the IO/PSL table, match the waist in the pockel cells to the waist of the mode cleaner, use standard optics available through a vendor, and offer a wide range of adjustment. The parameters are given in Table 24.

The adjustablility of the telescope can be seen in Figure 22. This shows that the telescope can adjust for changes in waist position due to shifts in optical path length of more than 15 cm while holding the waist size constant. It can also adjust for changes in waist size in either the MC waist or the waist in the pockel cell of 10% easily. The spot size on all the lenses is about 2 mm, making the optic relatively slow, keeping aberrations to a minimum. A major advantage to this design is that we have made the lenses in both the 4k and the 2k machine the same without sacrificing flexibility.

Table 24: Mode matching into 2k MC

Parameter	*Value*
Waist size in center of second Pockel cell	0.0396 mm
Distance to MML_1 from waist in Pockel cell	213.65 cm
Distance from MML_1 to MML_2	52.70 cm
Distance from MML_2 to MML_3	127.35 cm
Distance from MML_3 to MC waist	590.98 cm
Waist size in MC	0.1818 cm
Nominal focal length of MML_1 (focal length for 1064 nm)	100 cm (114.56 cm)
Nominal focal length of MML_2 (focal length for 1064 nm)	-100 cm (-114.56 cm)
Nominal focal length of MML_3 (focal length for 1064 nm)	300 cm (343.62 cm)

Figure 22: Adjustment of Mode Matching into 2k MC

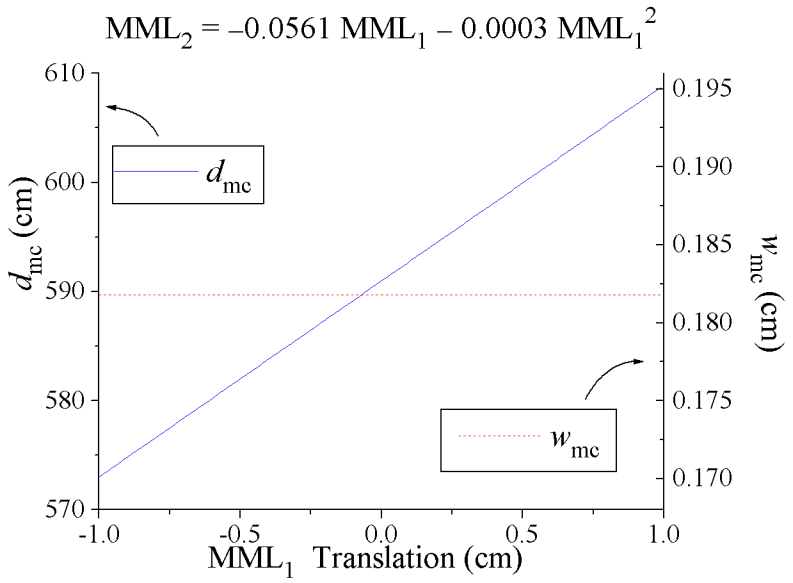

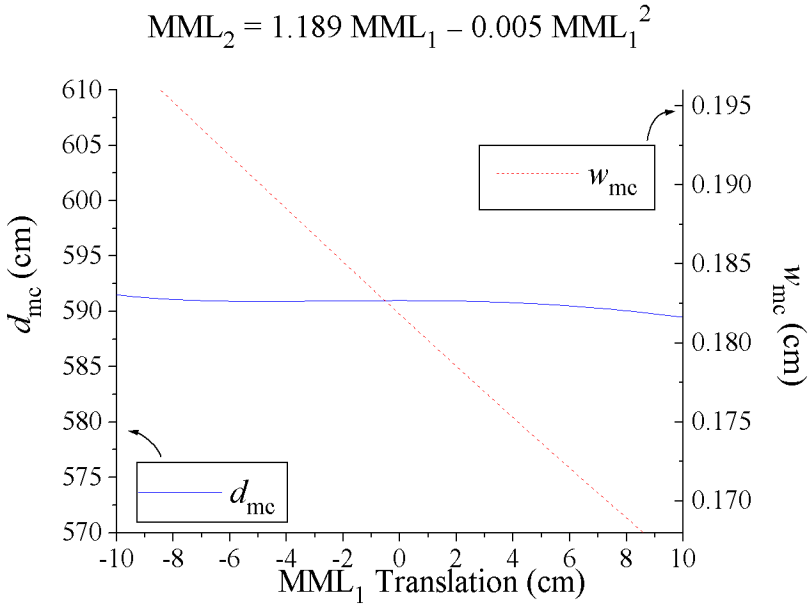

6.3. Mode cleaner performance.

6.3.1. Frequency Fluctuations

The MC will have the following frequency noise requirements at the given frequencies:

Table 25: Mode-cleaner noise performance.

Frequency	*Noise*
40 Hz	3×10^{-4} Hz/$\sqrt{Hz}$
100 Hz	1.5×10^{-5} Hz/$\sqrt{Hz}$
1000 Hz	1×10^{-5} Hz/$\sqrt{Hz}$

For more complete specifications, see "Mode Cleaner Length/Frequency Control Design"[1].

6.3.2. Rejection of the higher order modes.

The value of $g = 0.29$ was chosen by considering the transmission of higher order modes. Figure 23 shows the electric field amplitude transmitted by the mode cleaner under the assumption that it is illuminated with single frequency light with many higher-order modes present in the beam. (In order to avoid having an excessive number of points, the calculation was done for a finesse of $F \approx 100$.) The amplitude of the higher-order modes in the input beam was assumed to fall as $1/\sqrt{l+m}$. In addition, the finite size of the coating on the curved mirror was taken into account in the following way. The linear size of higher-order modes follows $\sqrt{l \times m}$. For the size of the coating on the curved mirror, this means that modes with index bigger than 5 will spill over the high-reflectance area at the 200 ppm level, leading to an effective reduction in the finesse of the cavity. We assumed that modes with ($l+m > 10$) would suffer this loss, initially as $1/\sqrt[4]{l+m}$ up to $l+m = 15$, as $1/\sqrt{l+m}$ up to $l+m = 20$, and as $1/(l+m)$ thereafter.

The large isolated peak at $g = 0.25$ is from the TEM_{21} and TEM_{30} modes. Other strong peaks include $l+m = 5$ at $g = 0.096$, $l+m = 7$ at $g = 0.38$, and $l+m = 4$ at $g = 0.5$.

The modes are quite crowded for some values of g and rather sparse for others. In particular, there are is a relatively wide gap on either side of the peak at $g = 0.25$. The operating point was chosen

1. *Mode Cleaner Length/Frequency Control Design,* P. Fritschel, N. Mavalvala, D. Ouimette, LIGO-T970218-01-D

in this gap; g was chosen larger than 0.25 so that thermal effects, which will tend to increase the radii of curvature, move the mode cleaner away from the strong maximum at g = 0.25. For circulating power of 4 kW, we estimate that the sagitta of the MC cavity mirrors will change by ~0.1 nm, corresponding to a change of the cavity g-factor from 0.290 (0.291) to 0.291 (0.292) for the 4 km (2 km) MC.

Because the calculation was done for F = 100, the transmission at the operating point in Figure 23 is higher than for the high finesse the mode cleaner will have. The computed transmission for key modes for F = 1550 is:

- TEM_{01}, TEM_{10}: 0.0012 in amplitude, 1.4 ppm in intensity.
- TEM_{30}, TEM_{21}: 0.0043 in amplitude; 18 ppm in intensity.

Figure 23: Higher Order Mode Transmission of 4 km IFO

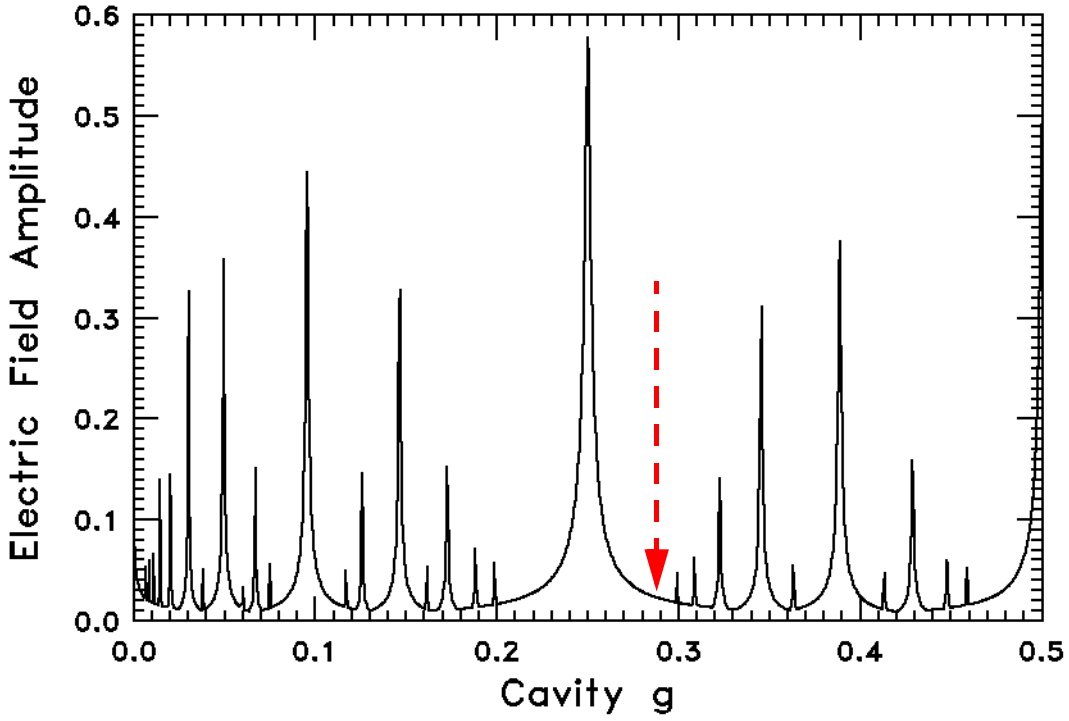

6.3.3. Wiggle and noise suppression.

Beam wiggle will be suppressed by a factor of typically 600 by the mode cleaner. Above the corner frequency of 6 kHz, laser noise is suppressed as 1/*f*.

6.3.4. Mode Cleaner Length and Alignment Requirements

6.3.4.1 Allowable sideband detune from resonance

Allowable sideband detune from resonance: 100 Hz

This requirement was derived to hold RF oscillator phase noise to amplitude modulation after the mode cleaner at the level of 10^{-8} / rHz[1]. For a given modulation frequency, this sets the initial length position tolerance.

6.3.4.2 Mode Cleaner Alignment

- Low frequency: beam jitter -> frequency noise must be kept below mode cleaner thermal noise, requiring $\theta_{rms} < 3 \times 10^{-7}$ rad[2] (at 100 Hz). This requirement is met by the mode cleaner ASC system.

6.3.4.3 Mode Cleaner Beam Centering

- The beam spot must be centered in the mode cleaner mirrors to a precision of 3 mm to avoid length-misalignment couplings.[3] This sets the initial angular position tolerance.

6.3.4.4 Initial Optics Positioning Requirements

These requirements sets the positioning tolerance of the 2 km and 4 km MC as follows:

Table 26: Mode Cleaner Alignment Requirements

Parameter	*Value*	*Tolerance*
2 km MC Half Cavity Length	15.251 m	**+/- 1000 μm**
2 km Angular Tolerance		**+/- 200 μrad**
4 km MC Half Cavity Length	12.240 m	**+/- 1000 μm**
4 km Angular Tolerance		**+/- 200 μrad**

6.3.5. Alignment Procedure

The initial alignment will begin with the installation of the in-vacuum chamber components. For the mode cleaner, we will need to know the separation of the tables in HAM7-8 and HAM1-2 to 1 mm. ASC is to provide position information in the chambers, such that a fiducial point on an optical component can be located to this distance. (The distance between the inside edges of the tables at two points separated by the diameter of the beam tube connecting them would be the most convenient.) Once this position is known, the following procedure will be used (Although we specify 2 km MC alignment procedures here; the method is applicable to the 4 km IFO):

1) The PSL will provide a 50 mW beam to the IOO which will be directed into the HAM7 through viewport WH7B2F3. The steering mirror SM1 into the MC will be placed to within 3 mm of its specified position using dead reckoning.

1. Length Sensing and Control Design Requirements Document, T960058
2. see (2) above
3. Alignment Sensing and Control Requirements Document, LIGO-T952007-03-I

2) The MC1 SOS (flat) will then be placed in its specified position to within 1 mm and 200 μrad using specially designed tooling (either CTI or UF tooling pending outcome of CTI prototyping for the LOS). Similarly MC3 (flat) will be placed in its specified positions with 1 mm and 200 μrad accuracy.

3) To achieve the appropriate mode cleaner length, MC2 will be positioned to within 1 mm of the specified length. This will be accomplished using the ASC fiducial measurement.

4) A pilot beam (> 50 mW He-Ne laser) mode-matched to the PSL IR beam located outside HAM7 will be directed though the rear of SM1 to toward MC1. (See Figure 24.) Alignment jigs (Figure 25) placed between SM1 and MC1 and on the beamline reflected by MC1 will be used to overlap the the reflected pilot beam to the IR beam to within 200 μrad by separating them a distance of 5 m (using the in HAM folding mirrors to send the beam to a photodiode located on IOT7 outside the HAM).

5) Approximately 85% of the pilot beam is transmitted through each MC optic. The first transmitted pilot beam will be directed to MC3. Using SOS alignment tooling (Figure 26, Drawing LIGO-D980197-00-D), the foward propagating beam will be positioned in the center of MC3 to within 1 mm by moving MC3 into position.

6) Using the DC ASC inputs to the MC3 SOS actuators, the pitch and yaw of MC3 will be adjusted to deliver the reflected beam to MC2 on HAM8. Again, SOS beam positioning tooling will be used to position the center of MC2 to within 1 mm.

7) MC2 will then be adjusted using SOS actuators to retroreflect the beam back (counterpropagate) to MC3 and MC1.

8) MC1 will be adjusted using SOS actuators to steer this counterpropagating beam down to the center of MC2.

9) Once the counterpropagating beam (as well as the propagating beam) has been centered on MC2, MC2 will be adjusted in pitch and yaw to bring the foward propagating beam onto the center of MC1 and aligned such that the signal in the photodiode is maximized. This defines the mode cleaner cavity to within 200 μrad and length to within 1 mm.

8) At this point, the alignment jigs and positioning tooling will be removed. The alignment tolerances of 200 μrad and 1 mm should be adequate to achieve lock. It is anticipated, however, that vacuum pumpdown of the HAMs will shift the stacks by as much as 2 mm and will cause some misalignment of the MC. The pilot beam will remain to allow re-adjustment of the MC2,3 pitch and yaw to regain the necessary alignment tolerance. At this point the MC should be locked.

9) Once lock is achieved, the WFS will align the MC to the required locked angular alignment. A measurement of the FSR of the MC will be performed to determine the length. If the measurement indicates that the pump down shifts have pushed the mirrors beyond the range of the SOS actuators, HAM8 will be re-opened and MC2 repositioned to compensate for the shift. Pump and lock will proceed as in 8).

Figure 24: Mode Cleaner Initial Alignment

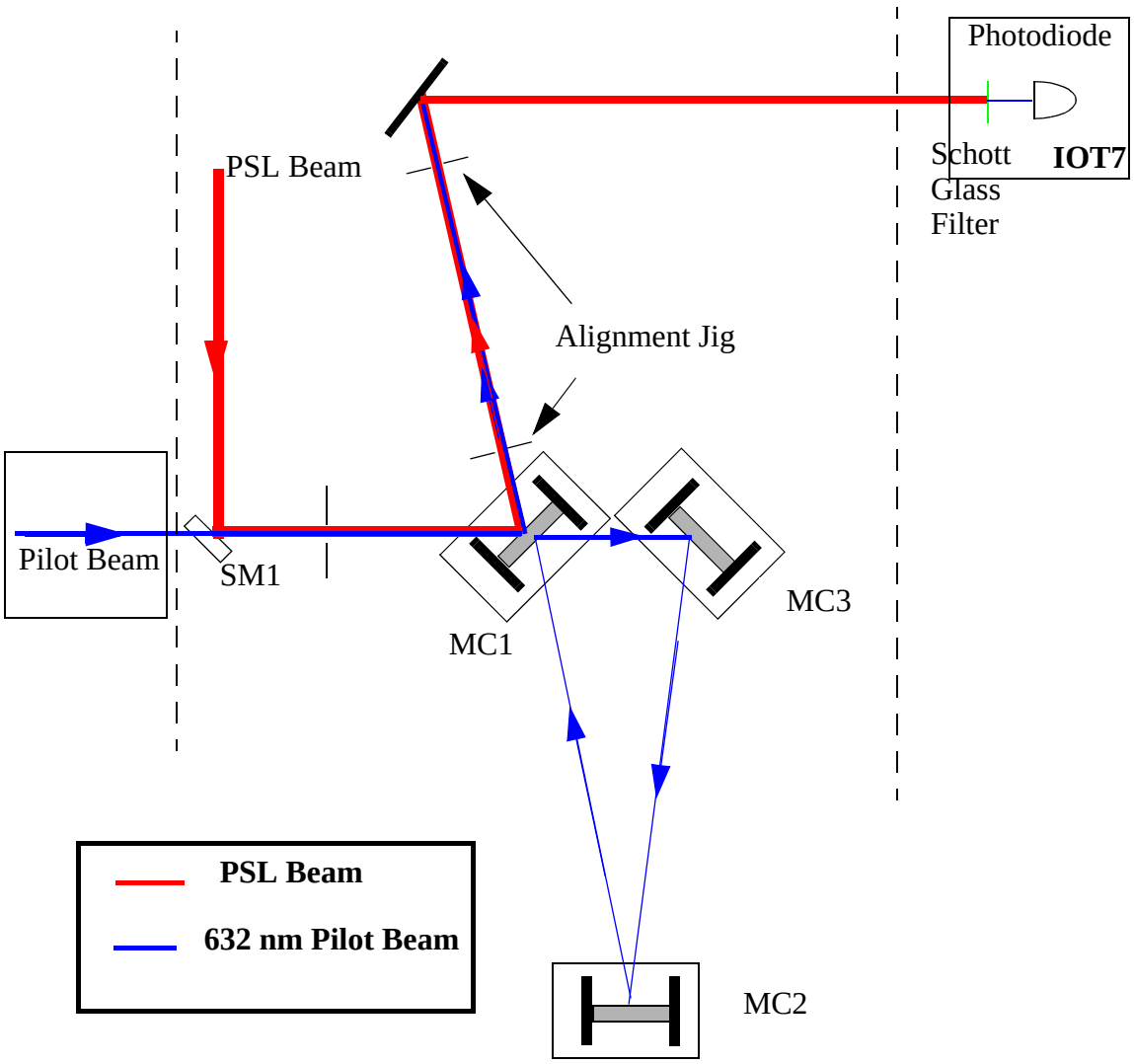

Figure 25: MC Alignment Jigs

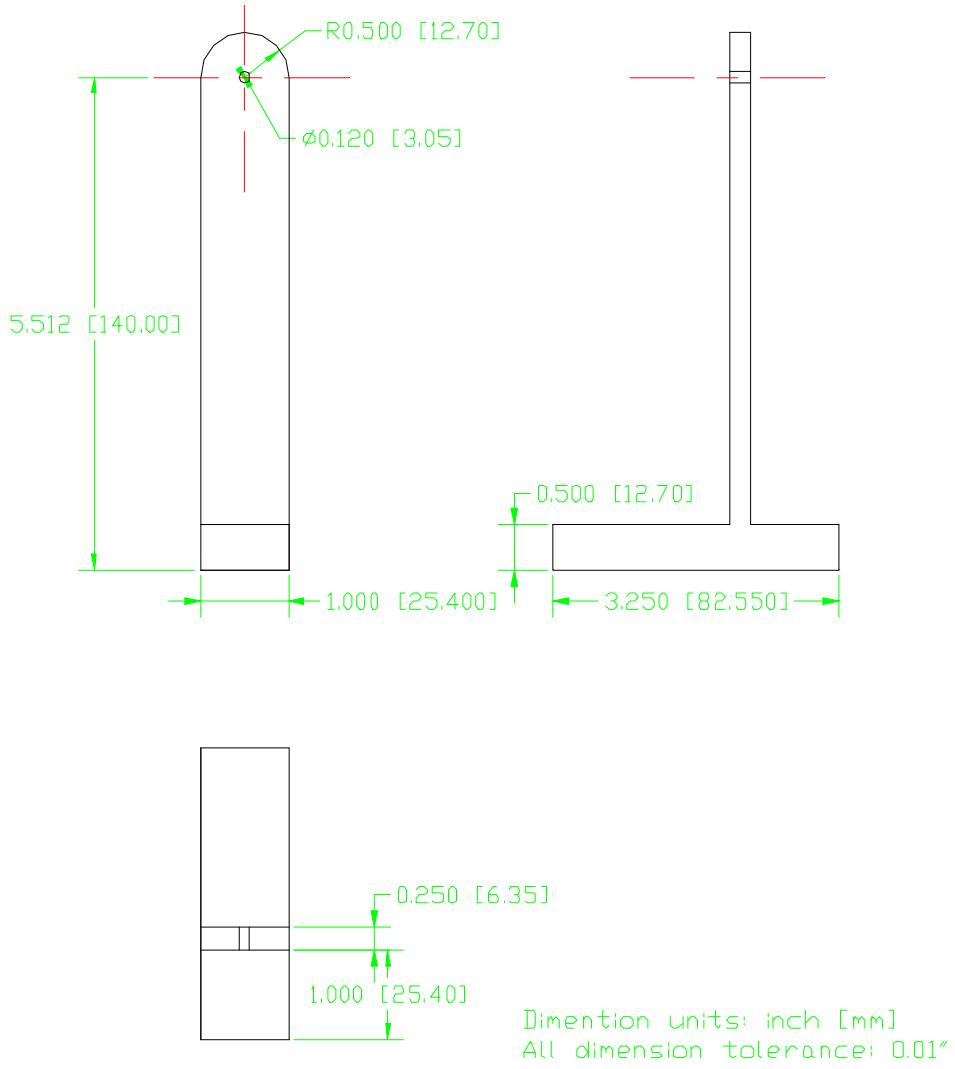

Figure 26: SOS Centering Tool

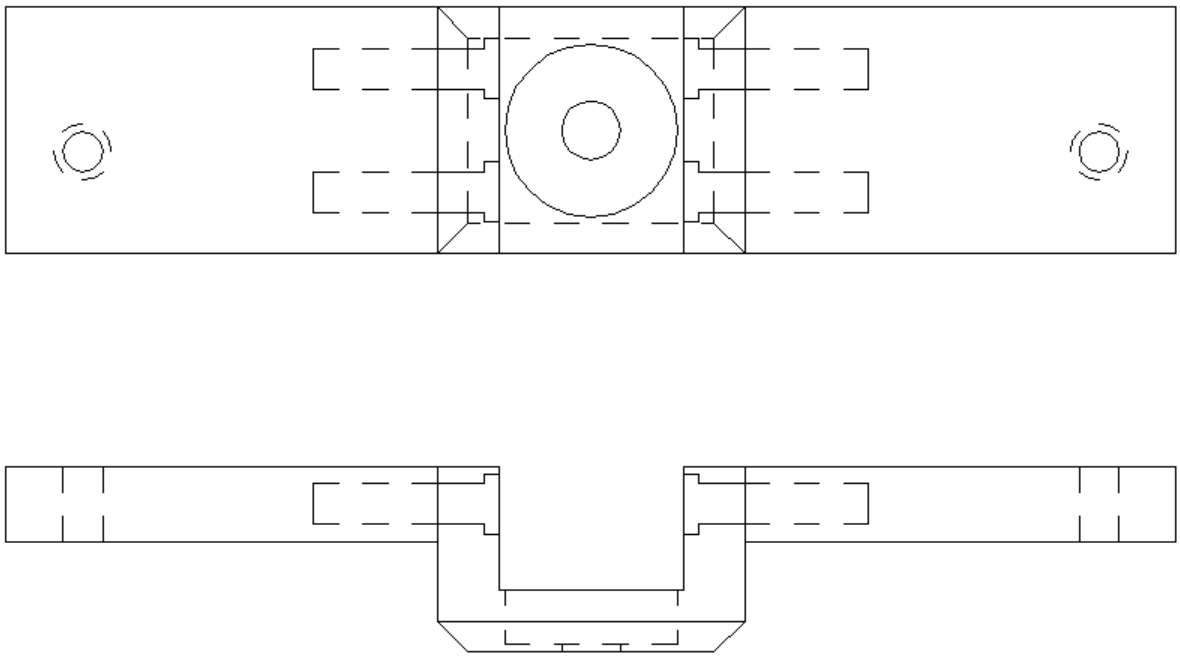

7 IFO MODE MATCHING TELESCOPE

7.1. Final Optical Design

The LIGO IFO mode matching telescopes (MMT) will use a three element reflective spherical mirror design. Our design allows for optimization of mode-matched power by having independent adjustment of two degrees of freedom (waist size and position or, alternatively, wavefront radius of curvature and beam divergence angle) over a wide range of modal space.

The design philosophy is governed by the following criteria:

- Minimize the number of optics after the mode cleaner.
- Limit beam aperturing to the 1 ppm Gaussian intensity contour for direct path scattering
- Adjustment of the mode parameters in the IFO sufficient to meet the 95% coupling requirement when all know deviations are taken into account.
- Minimize astigmatism introduced into the beam.
- Allow for steering of the beam into the mode IFO without significant higher order modal con-

tamination.

Figure 27 shows the conceptual layout and definition of parameters. Table 27 lists the input parameters used in our design.

Figure 27: Definition of Parameters

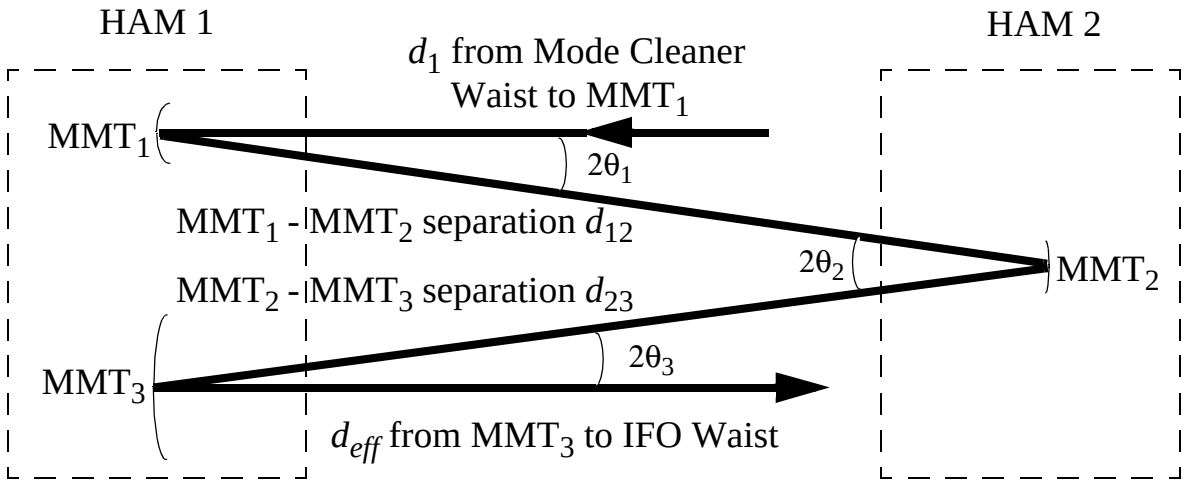

Analytical details of the design can be found in *Design Considerations for LIGO Mode-Matching Telescopes, LIGO-T970143-00-D*. Briefly, we analytically solve for *all* possible radii of curvature (R_{MMT1}, R_{MMT2}, R_{MMT3}) which mode-match to the Fabry-Perot cavity. We then use optimization to select the set which provides the *maximum* amount of adjustment of waist size and position in the core optics. The optimal values for (R_{MMT1}, R_{MMT2}, R_{MMT3}) for both the 2 km and the 4 km IFO are shown in Table 27.

Table 27: Parameters for the 4 and 2km IFO

	Units	4k	2k
w_0 = Waist size in Mode Cleaner	cm	0.1629	0.1818
d_1 = Distance from mode cleaner waist to MMT$_1$	m	1.436	3.159
d_{12} = Distance from MMT$_1$ to MMT$_2$	m	13.72	13.41
d_{23} = Distance from MMT$_2$ to MMT$_3$	m	14.45	13.78
d_{rm} = Distance to recycling mirror	m	16.18	17.22
w_{eff} = Effective waist size in arms	cm	3.16	2.94
d_{eff} = Effective waist position in arms	m	1692	1161
w_3 = Waist size in arm	cm	3.51	2.56
d_3 = Waist position in arm from ITM	m	975	615.8
θ_1 = Incident angle on MMT$_1$	mrad	71.6	96.2

θ_2 = Incident angle on MMT_2	mrad	6.8	13.2
θ_3 = Incident angle on MMT_3	mrad	5.9	6.8
w_{m1} = Spot size on MMT_1	cm	0.169	0.195
w_{m2} = Spot size on MMT_2	cm	0.365	0.302
w_{m3} = Spot size on MMT_3	cm	3.65	3.23

7.1.1. 2 km IFO

7.1.1.1 Optical Component Specifications

General optical component specifications for the 2 km MMT1, MMT2, and MMT3 mirrors are given in Table 28, Table 29, and Table 30.

Detailed specifications for the mirror blanks can be found in LIGO-D970533,34,35. (incorrectly assigned D numbers)

Detailed CAD drawings for the mirror blanks can be found in LIGO-D970536,37,38

Detailed specifications for the substrates can be found in LIGO-E970146,44,43.

Detailed CAD drawings for the substrates can be found in LIGO-D970589,87,86

Table 28: 2 km MMT1 Specifications

	Value	Tolerance
Substrate Material	Fused Silica	
Front Surface Radius of Curvature	11.28 m	$\pm 0.1m$
Diameter	75.0 mm	+ 1 mm, - 0 mm
Thickness (thick side)	25. 0 mm	+ 0 mm, - 0.5 mm
Wedge Angle / orientation	30 min thick side down	+ 10 min, -0 min
Transmittance	50 ppm	+ 0 ppm, - 50 ppm
Clear Aperture	60 mm	

Table 29: 2 km MMT2 Specifications

	Value	Tolerance
Substrate Material	Fused Silica	
Front Surface Radius of Curvature	2.1 m	$\pm 0.04 m$
Diameter	75.0 mm	+ 1 mm, - 0 mm
Thickness (thick side)	25. 0 mm	+ 0 mm, - 0.5 mm
Wedge Angle / orientation	30 min thick side down	+ 10 min, -0 min
Transmittance	50 ppm	+ 0 ppm, - 50 ppm
Clear Aperture	60 mm	

Table 30: 2 km MMT3 Specifications

	Value	Tolerance
Substrate Material	Fused Silica	
Front Surface Radius of Curvature	25.16 m	$\pm 0.025 m$
Diameter	250.0 mm	+ 1 mm, - 0 mm
Thickness (thick side)	100.0 mm	+ 0 mm, - 0.5 mm
Wedge Angle / orientation	2 deg 0 min thick side up	+ 10 min, -0 min
Transmittance	50 ppm	+ 0 ppm, - 50 ppm
Clear Aperture	60 mm	

7.1.1.2 Mode-Matching Diagram

Figure 28 displays the capability of the 2 km MMT to accommodate combined deviations from

- Thermal Distortions in COC, MC, and FR
- Surface Figure Focus Error Due to Imperfect Polishing in the COC, MC, FI, and MMT optics
- Pump Down Shifts and Stack Drift

Of these, the dominant errors come from thermal lensing in the FR and surface figure focus error in MMT3.

Figure 28: Mode Matching Diagram for the 2 km IFO

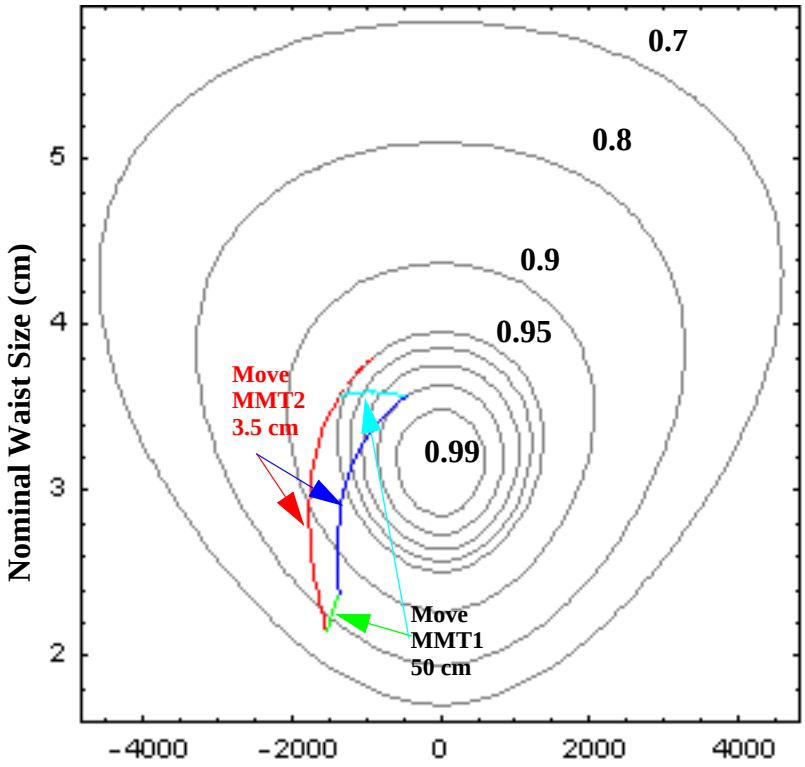

7.1.1.3 Suspensions for the 2-km MMT

The mode-matching telescope employs Small Optic Suspensions for MMT1 and MMT2.(The two Steering Mirrors are in identical SOS's.) The suspensions are described in Small Optics Suspensions Final Design, S. Kawamura, LIGO-T970135-02-D. MMT3 is placed in a Large Optic Suspension supplied by SUS. The electronics that drive the suspensions are designed to the requirements shown in Table 31.

Table 31: SOS/LOS Parameters for the 2-km MMT

Parameter	*Suspension*	*Value*
Length Dynamic Range	SOS	500 μm pk-pk
Angular Dynamic Range	SOS	>5 mrad pk-pk
Noise	SOS	5×10^{-16} m/rtHz
Length Dynamic Range	LOS	40 μm pk-pk
Angular Dynamic Range	LOS	1 mrad pk-pk
Noise	LOS	5×10^{-16} m/rtHz

7.1.1.4 Risers for MMT2 (2K)

The beam height enters the core optics at a height of +45 mm in the LIGO Global Coordinate system The plane of the mode cleaner is at -57 mm in the LIGO Global Coordinate system. This difference requires that the beam be directed slightly upwards by the MMT. We step the beam up half MMT1 and MMT2 and the rest between MMT2 and MMT3. The riser is a solid block 51 mm in height with provision to clamp the SOS to it and to clamp the riser to the HAM table.

7.1.2. 4 km IFO

7.1.2.1 Optical Component Specifications

General optical component specifications for the 2 km MMT1, MMT2, and MMT3 mirrors are given in Table 33, Table 34, and Table 34.

Detailed specifications for the mirror blanks can be found in LIGO-D970533,34,35. (incorrectly assigned D numbers)

Detailed CAD drawings for the mirror blanks can be found in LIGO-D970536,37,38

Detailed specifications for the substrates can be found in LIGO-E970146,44,43.

Detailed CAD drawings for the substrates can be found in LIGO-D970589,87,86

Table 32: 4 km MMT1 Specifications

	Value	Tolerance
Substrate Material	Fused Silica	
Front Surface Radius of Curvature	6.76 m	$\pm 0.035 m$
Diameter	75.0 mm	+ 1 mm, - 0 mm
Thickness (thick side)	25.0 mm	+ 0 mm, - 0.5 mm
Wedge Angle / orientation	30 min thick side down	+ 10 min, -0 min
Transmittance	50 ppm	+ 0 ppm, - 50 ppm
Clear Aperture	60 mm	

Table 33: 4 km MMT2 Specifications

	Value	Tolerance
Substrate Material	Fused Silica	
Front Surface Radius of Curvature	3.16 m	$\pm 0.06 m$
Diameter	75.0 mm	+ 1 mm, - 0 mm

Thickness (thick side)	25. 0 mm	+ 0 mm, - 0.5 mm
Wedge Angle / orientation	30 min thick side down	+ 10 min, -0 min
Transmittance	50 ppm	+ 0 ppm, - 50 ppm
Clear Aperture	60 mm	

Table 34: 4 km MMT3 Specifications

	Value	Tolerance
Substrate Material	Fused Silica	
Front Surface Radius of Curvature	25.16 m	$\pm 0.025 m$
Diameter	250.0 mm	+ 1 mm, - 0 mm
Thickness (thick side)	100.0 mm	+ 0 mm, - 0.5 mm
Wedge Angle / orientation	2 deg 0 min thick side up	+ 10 min, -0 min
Transmittance	50 ppm	+ 0 ppm, - 50 ppm
Clear Aperture	60 mm	

7.1.2.2 Mode-Matching Diagram

Figure 29: Mode Matching Diagram for the 4 km IFO

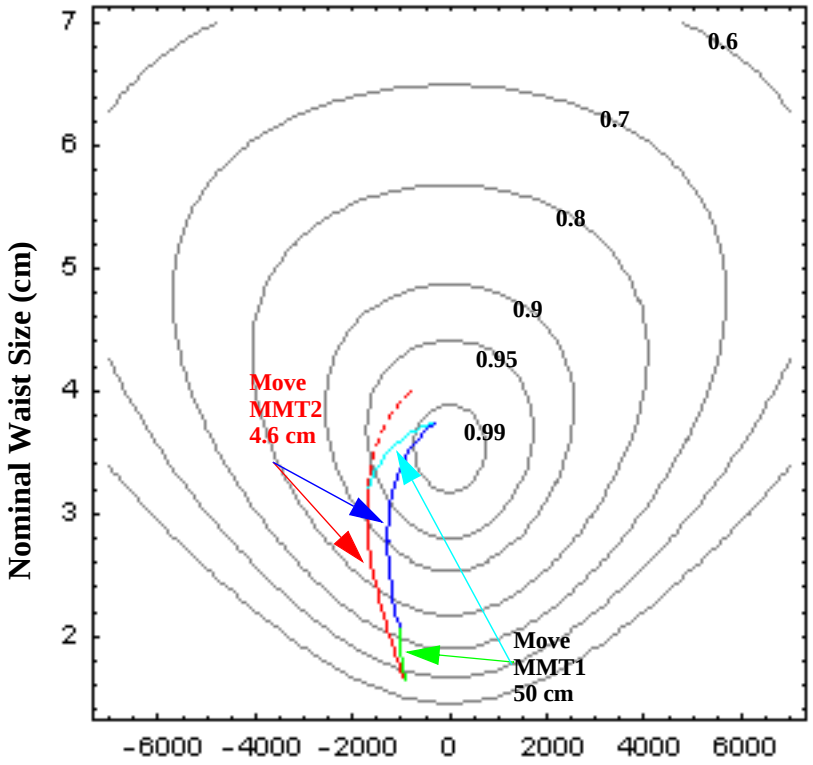

7.1.2.3 Suspensions for the 2-km MMT

The mode-matching telescope employs Small Optic Suspensions for MMT1 and MMT2.(The Steering Mirror is in an identical SOS.) The suspensions are described in Small Optics Suspensions Final Design, S. Kawamura, LIGO-T970135-02-D. MMT3 is placed in a Large Optic Suspension supplied by SUS. The electronics that drive the suspensions are designed to the requirements shown in Table 35.

Table 35: SOS/LOS Parameters for the 2-km MMT

Parameter	*Suspension*	*Value*
Length Dynamic Range	SOS	500 µm pk-pk
Angular Dynamic Range	SOS	>5 mrad pk-pk
Noise	SOS	5×10^{-16} m/rtHz
Length Dynamic Range	LOS	40 µm pk-pk

Parameter	*Suspension*	*Value*
Angular Dynamic Range	LOS	1 mrad pk-pk
Noise	LOS	5×10^{-16} m/rtHz

7.1.2.4 Risers for MMT2 (4K)

The beam height enters the core optics at a height of +27.8 mm in the LIGO Global Coordinate system The plane of the mode cleaner is at -57 mm in the LIGO Global Coordinate system. This difference requires that the beam be directed slightly upwards by the MMT. We step the beam up half MMT1 and MMT2 and the rest between MMT2 and MMT3. The riser is a solid block 42 mm in height with provision to clamp the SOS to it and to clamp the riser to the HAM table.

7.2. Alignment Protocol and Tooling

7.2.1. Initial Positioning of the MMT Optics

Initial positioning of the MMT optics will be accomplished in a manner similar to MC optics. Initial alignment tolerances are shown below.

Table 36: Initial MMT Alignment Tolerance

Element	*Centering Requirement*	*Position Requirement*
MMT1	3 mm	1 cm
MMT2	3 mm	1 mm
MMT3	3 mm[a]	1 mm

a. ASC requirement for recycling mirror centering

7.2.2. Tooling

Because positioning tolerances are fairly loose, the initial positioning of the MMT within the HAM stacks will be accomplished using the tooling used in the MC optics for MMT1,2. Tooling designs are found in:

1) MMT1 Center Alignment Tool for 4k Machine (LIGO-D980195-00-D)

2) MMT2 Center Alignment Tool for 4k Machine (LIGO-D980196-00-D)

3) MMT1 Center Alignment Tool for 2k Machine (LIGO-D980197-00-D)

4) MMT2 Center Alignment Tool for 2k Machine (LIGO-D980198-00-D)

5) MMT Mounting Alignment Tool (LIGO-D980199-00-D)

6) Assembly Drawing for MMT Alignment Tool (LIGO-D980207

7.2.3. Alignment within the IOO

For the MMT, we will need to know the separation of the tables in HAM7-8 and HAM1-2 to 1 mm. As with the mode cleaner, ASC is to provide position information in the chambers, such that a fiducial point on an optical component can be located to this distance. Once this position is known, the following procedure will be used (Although we specify 2 km MMT alignment procedures here; the method is applicable to the 4 km MMT):

1) From the fiducial data, MMT1, 2, and 3 will be positioned to within 1 mm of their specified positions using CTI tooling (for MMT3) or UF tooling (MMT1,2). The steering mirror (MMT injection) will also be placed.

2) The PSL will provide a 50 mW beam to the IOO which will be directed into the HAM7 through viewport WH7B2F3. Most of the beam will be directed toward IOT7 (since the MC is unlocked).

3) A pilot beam (> 50 mW He-Ne laser) mode-matched to the PSL IR beam located outside HAM7 will be directed though the rear of SM1 to toward MC1. As detailed in Section 6.3.4, the pilot beam will aligned to the PSL beam to an accuracy of 200 μrad.

4) Centering tooling will be placed on MMT1 and 2 SOSs. (See Figure 25).

5) The pilot beam transmitted through the MC mirrors will be reflected off the MMT injection mirror. The Faraday isolator will be positioned at this time. The DC ASC input to the MMT injection mirror actuator will be used to adjust the pitch and yaw of the mirror such that the beam is positioned on MMT1 to within 1 mm of center. The adjustment will be locked.

6) The MMT1 SOS will then be adjusted in pitch and yaw using DC ASC inputs to the SOS to position the beam on MMT2 to within 1 mm of center. The adjustment will be locked.

7) The steering of the beam to the final mirror MMT3 is complicated by the fact that the spot size on MMT3 is 3.2 cm. However, if the positions of MMT2 and 3 are known to an accuracy of 1 mm to a fiducial reference, the beam

8) Once the beam is centered on MMT3, ACS will use the specified alignment procedure[1] for aligning MMT3 to the COC.

1. Ken Mason, “ASC Initial Alignment Procedures -2k Interferometer” LIGO-T970151

Figure 30: MMT Initial Alignment

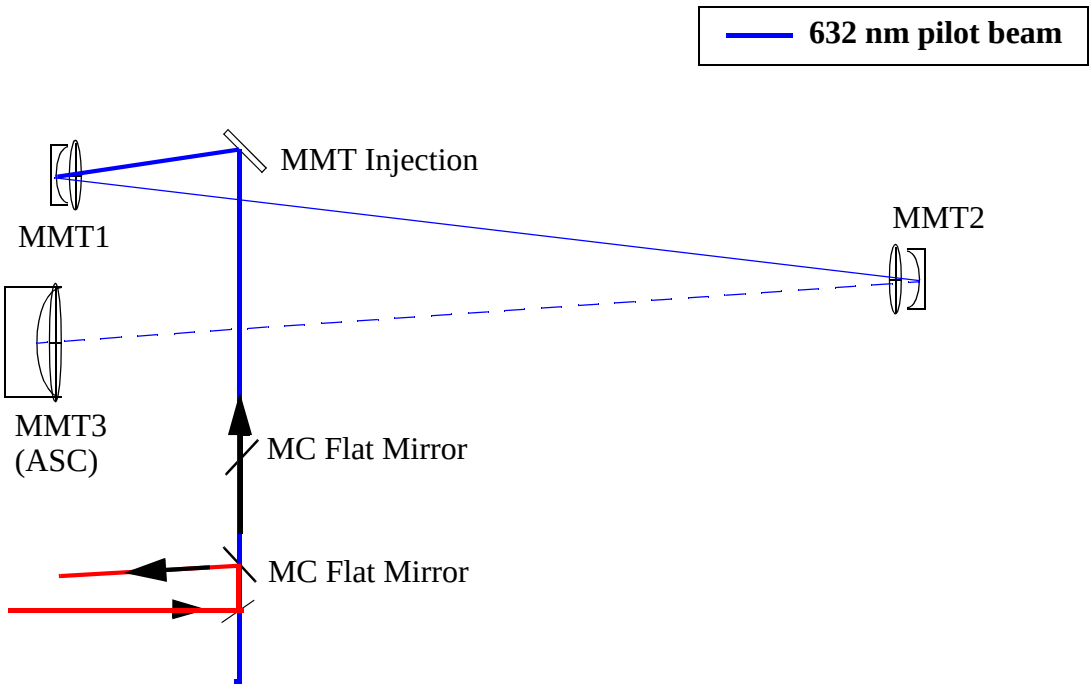

8 OPTICAL THROUGHPUT

The IOO must deliver 75% of the TEM_{00} light emerging from the PSL to the IFO, including all integrated losses from reflection, transmission, and absorption in the IOO optical components. The following table shows the transmission of the components of the IOO components. Numbers are rounded to 3 digits. For the suspended components we have assumed coatings comparable to those of the core optics, with 30 ppm loss on reflectance. The small optics are assumed to have antireflection coatings that match the Ealing narrowband multilayer coatings (0.1%). The largest individual loss comes from the large Faraday isolator, where the polarizing components contribute to a total loss of 8%. We gain considerably from the elimination of the first Faraday isolator that was in the conceptual design.

Table 37: Optical efficiency of IOO system

Item	*Loss(%)*	*Transmittance*	*Accumulated Transmittance*
RF modulation core optics	1.5	0.985	0.985
RF for mode cleaner	1.0	0.990	0.975
3 mode matching lenses	0.6	0.994	0.970
HAM1 window	0.2	0.998	0.968
3 beam steering mirrors	0.06	0.999	0.997
Mode cleaner	5	0.950	0.919
Faraday isolator	8	0.920	0.845
Mode matching telescope (4 mirrors)	0.45	0.996	0.841

9 DIAGNOSTICS

9.1. PSL/IOO Table

9.1.1. RF Amplitude Modulation Monitor

RF amplitude modulation of the laser beam after passing the EOMs will be monitored of line by a fast photodiode. The signal will be fed to a RF spectrum analyzer. The dc signal from the photodiode will also be monitored. The ratio of the RF signal at the three modulation frequencies will be compared with dc signal to calculate the amount of residual RFAM.

9.1.2. RF Sideband Monitor

RF sidebands generated by the EOMs will be monitored off line with either a Burleigh CF(T)-500S-NIRoptical spectrum analyzer or similar model.. The resolution of the optical spectrum analyzer is about 1.5 MHz. To distinguish the smallest sidebands from the tail of the carrier, the temporal signal will be recorded by a digital oscilloscope and read to a computer. A fitting procedure will be used to calculate the intensities of the sidebands.

9.1.2.1 PSL Table

An optical spectrum analyzer will be located on the PSL table for monitoring sidebands before the mode cleaner.

9.1.2.2

An optical spectrum analyzer will be located on the IOT table for monitoring sidebands after the mode cleaner.

9.2. Mode Cleaner Diagnostics

Taken care of by ISC. Refer to LIGO-T970218-01-D

9.3. Mode Matching Wavefront Sensing

9.3.1. Introduction

LIGO requires optimal coupling of the TEM_{00} mode to the Fabry-Perot arms of the interferometer in order to meet requirements for strain sensitivity and to suppress quantum shot noise on the photodetector. To meet these requirements, a three-element all-reflective mode-matching telescope has been designed to maximize the TEM_{00} power coupling.[1] Here, we propose a design for a mode-matching wavefront sensor to serve as a diagnostic for the mode matching optics.

9.3.2. Mode Matching Wave Front Sensor

9.3.2.1 “Bullseye” Mode

Assuming the resonant cavity is perfectly aligned with respect to the input laser but is slightly mode-mismatched, the input beam is then decomposed into eigenmodes of the cavity and the beam reflected from the cavity contains high order cylindrical modes which are not resonant with the cavity. In the limit of small mismatching, only decomposition into the lowest order cylindrical modes is significant. The decomposition of input beam TEM_{00} mode $V'_0(r, z)$ into cavity modes can be written as[2]

1. T. Delker, R. Adhikari, and D. Reitze, “Design Considerations for LIGO Mode-Matching Telescopes”, *LIGO-T970143-00-D*
2. Dana Z. Anderson, “Alignment of Resonant Optical Cavities”, Applied Optics, Vol. 23, No. 17, 2994 (1984), and references therein.

$$V'_0(r,z) \cong CV_0(r,z) + \varepsilon V_1(r,z) \quad . \tag{1}$$

where C and ε are decomposition coefficients, and $V_0(r, z)$ and $V_1(r, z)$ are the two lowest-order Laguerre-Gaussian modes of the cavity.

$$V_0(r,z) = \sqrt{\frac{2}{\pi}}\frac{1}{w}\exp\left[-r^2\left(\frac{1}{w^2} + i\frac{\pi}{\lambda R}\right)\right] \tag{2}$$

$$V_1(r,z) = \sqrt{\frac{2}{\pi}}\frac{1}{w}\left(1 - 2\frac{r^2}{w^2}\right)\exp\left[-r^2\left(\frac{1}{w^2} + i\frac{\pi}{\lambda R}\right)\right]. \tag{3}$$

Here, both waist size w and wave front radius of curvature R are functions of propagation distance z along the beam. $V_1(r, z)$ has an intensity pattern of bullseye type. There are two independent type of mismatches: mismatch of waist size and mismatch of waist position. For small mismatches,

$$C = 1 - i\frac{b}{2z_R} \tag{4}$$

and ε and its real and imaginary parts are defined as

$$\varepsilon = \varepsilon' + i\varepsilon'' = -\left(\frac{w'_0}{w_0} - 1\right) - i\frac{b}{2z_R} \quad , \tag{5}$$

where w'_0 and w_0 are the waist sizes of the input beam and the cavity mode waist size, respectively; b is the displacement of input beam waist position relative to the cavity mode waist position along the cavity axis; z_R is the Rayleigh length of the cavity mode and λ is the wavelength of the laser. If we measure the coupling coefficient, the mismatches of beam parameters can be readily obtained.

9.3.2.2 The "Bullseye" Shape Photodiode

The "bullseye" mode has a null point radially at $r = R_0 = w/\sqrt{2}$ so a bullseye type of differential sensor, a photodiode design with an inner disk and outer ring, is suitable for detecting this mode using RF heterodyne detection[1]. Assuming a radius R_0 which separates inner disk from the outer ring, and assuming the sidebands and the high order modes are totally rejected by the cavity, the heterodyne signal generated by back-reflected light on the bullseye detector can be calculated to give

$$S_{bull'\text{s eye}} = KP|\varepsilon|J_0(\delta)J_1(\delta)(1 - R_{00}^{carrier})\sin(2\psi + \alpha)\cos(\phi) \quad , \tag{6}$$

where K is a proportional factor which takes into account of the fraction of reflected optical power being detected by the bullseye photodiode and the efficiency of the photodiode, P is the incident

1. See the footnote of previous page and Daniel Sigg, "*Modal Model Update 4, Mode Mismatch*", LIGO Technical Note, LIGO-T960116-00-D, (1996)

power to the cavity, J_0 and J_1 are the Bessel functions, δ is the modulation index, and $R_{00}^{carrier}$ is the effective reflectance of the cavity for the carrier of the fundamental cavity mode which is resonant with the cavity; ψ is the Guoy phase measured from the cavity waist to the detector, ϕ is the phase of RF local oscillator, and α is the phase of the coupling coefficient ε defined as $\alpha = \mathrm{atan}(\varepsilon''/\varepsilon')$. For a critically coupled cavity, as in LIGO the recycling cavity, the reflectance $R_{00}^{carrier}$ should be small when the cavities are brought into resonance with the laser and can be neglected.

9.3.3. Bullseye Photodiode design

For practical reasons in the photodiode design, the outer ring is segmented to 3 sections by 3 radial gaps. The are three purposes behind this design: a) it enables an electrode lead from the inner disk to pass through the gap, b) it fits into the existing 4-channel quad-photodiode head electronics, and c) it allows future development of a combined alignment and mode-matching detector. Figure 31 shows the photodiode design. The inner disk has a size of 3.14 mm^2 and the each outer segment has a size of 6.28 mm^2. The expected specifications, some of them estimations by the manufacturer, are listed below.

Figure 31: Bullseye Photodiode.

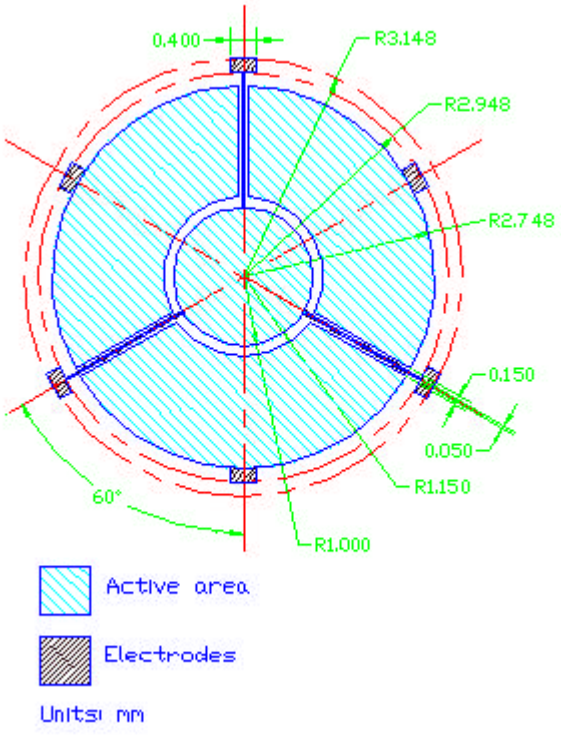

9.3.3.1 Specifications:

Inner disk active area: 3.14 mm^2.

Each outer segment active area: 6.28 mm^2.
Responsivity: >0.2 A/W at 1.064 μm.
Bias: <30 Volts.
Capacitance at 0 Volts bias: 75 pF for inner segment and 34 pF for each outer segment.
Capacitance at 25 Volts bias: 12 pF for inner segment and 5.5 pF for each outer segment.

9.3.4. MODE MATCHING ERROR SIGNAL AND DIAGNOSIS

9.3.4.1 Mismatching Signal, Waist Size and Waist Position

According to Equation (6), the mode matching error signal can be obtained by using two bullseye photodiodes at two Guoy phases ψ. When $2\psi = n\pi + \pi/2$, $\varepsilon' = |\varepsilon|\cos(\alpha)$ is measured; when $2\psi = n\pi$, $\varepsilon'' = |\varepsilon|\sin(\alpha)$ is measured, here n is an integer.

9.3.4.2 Proposed Mode Matching Diagnostics in LIGO

Mode matching in LIGO involves coupling between various cavities. Full treatment of mismatching in the vicinity of optimal mode matching has been developed by D. Sigg in a technical note[1]. Here we assume the mismatching between the recycling cavity and the arm cavities is not significant after the initial positioning of the core optics. The mode matching wavefront sensors provide information on the mismatch of the input beam and the recycling cavity.

In order to couple the maximum amount of the power from the PSL into the fundamental mode of the arm cavities, a mode matching telescope has been designed to steer and mode-match the beam. This is essentially a three-element telescope, using spherical, reflective optics. The current design has been optimized, within external constraints, to give maximum adjustablility of both the waist position and the waist size in the arm cavities. The mode-matching error can be measured by dithering the second telescope mirror (MMT_2), the most effective of the three telescope mirrors for dithering, and monitoring the error signal carried by the reflected light using two bullseye photodiodes. The error signal without dithering and the slope of the error signal measured by dithering MMT_2 altogether gives a measurement of waist size and waist position mismatches.

The dithering method can be achieved by driving MMT_2 longitudinally. The coupling coefficient can be calculated using parameters of current design of mode-matching telescope to give

$$\varepsilon = 6.3\Delta + i11\Delta \tag{7}$$

for 4-K interferometer and

$$\varepsilon = 7.4\Delta + i6.5\Delta \tag{8}$$

1. Daniel Sigg, "*Modal Model Update 4, Mode Mismatch*", LIGO Technical Note, LIGO-T960116-00-D, (1996)

for 2-K interferometer, where Δ is the displacement of MMT_2 in meters from a stationary position in the vicinity of optimal mode-matching. MMT_2 is supported by a Small Optics Suspension which can be magnetically driven within a dynamic range of 100 μm. This dynamic range of dithering results in a change in amplitude of the coupling coefficient of about 10^{-3}, which corresponds to a signal level of several tens of μW of light, taking into account the power sharing scheme with alignment sensing. This signal level is well beyond the shot noise limit. Once the mode-mismatch parameters are determined, then the necessary adjustments of the positions of two or three telescope mirrors can be made to optimize the mode matching. The relation between the coupling coefficient and the required adjustment of positions of MMT_1 and MMT_2, which are more suitable to be used for adjusting the mode matching after the initial alignment, can be derived to give,

$$\begin{bmatrix} x1 \\ x2 \end{bmatrix} = \begin{bmatrix} 13.3 & -7.64 \\ -0.369 & 0.122 \end{bmatrix} \begin{bmatrix} \varepsilon' \\ \varepsilon'' \end{bmatrix} \tag{9}$$

for 4-K, and

$$\begin{bmatrix} x1 \\ x2 \end{bmatrix} = \begin{bmatrix} 9.56 & -10.8 \\ -0.179 & -0.0496 \end{bmatrix} \begin{bmatrix} \varepsilon' \\ \varepsilon'' \end{bmatrix} \tag{10}$$

for 2-K interferometer. Here x1 and x2 are in meters and are the displacements moving away from each other from the optimal positions for MMT_1 and MMT_2, respectively.

9.3.4.3 Crosstalk of Mode Matching and Alignment Error Signals due to Tilting

The driving force imbalance in the MMT_2 control is about 1% which results in a tilt of magnitude 10μrad with 100 μm dithering. At a frequency of 0.1 Hz where the ASC gain is 100, this gives a tilt amplitude of order 0.01 at the mode match sensor. With a rejection factor of 100 of the donut sensor to a tilt wavefront, the effective tilt coupling is 10^(-3), which is a factor of 10 lower than the desired mode match error signal.

9.3.5. Guoy Phase Telescope Design

To acquire the correct Guoy phase while matching the beam size with the dimension of the bullseye photodiode for maximum sensitivity or maximum common mode rejection, a delicate telescope has to be used. A two-lens telescope can be used to achieve this purpose[1]. Here we use three-lens design to ease both the dependence of Guoy phase and the waist size at the detector on the position of the detector. Table 38 shows the results for the Guoy phase telescope design for 4-K and Table 39 for 2-K interferometer. The solutions are numerically exact but in reality the error of the Guoy phases and the waist sizes are determined by the tolerances of the focal lengths which are claimed by CVI Lasers to be less than 1%. Detailed error analysis will be present elsewhere. The slope of waist size is designed to be 10 μ*m*/cm at the detector where the slope of Guoy phase is about 0.05~0.09 degrees/cm. The nonzero slope of the waist size is designed for fine tuning of

1. N. Mavalvala, *"Alignment Issues in Laser Interferometric Gravitational-wave Detectors"*, Ph. D. Thesis, MIT (1997)

Table 38: Guoy Phase Telescope for 4-K interferometer. The Guoy Phases are measured from the effective waist position of the recycling cavity; the two waist sizes at the detector, 0.00141 m and 0.00170 m are for maximum sensitivity and optimal common mode rejection, respectively. The focal lengths of the lenses are chosen from the CVI catalog of fused silica single lenses and the numbers in the parentheses are nominal focal lengths in mm.
d1=the distance from the Faraday rotator to the first lens,
d12=the distance from the first lens to the second lens,
d23=the distance from the second lens to the third lens,
d34=the distance from the third lens to the bullseye photodiode**.**

Guoy Phase (Deg.)	*Waist at Detector (m)*	*Waist Slope at Detector (μm/cm)*	f_1(m)	f_2(m)	f_3(m)	d_1 (m)	d_{12} (m)	d_{23} (m)	d_{34} (m)
360	0.00141	10.0	-.2291 (-200)	.2291 (200)	-.0872 (-76)	3.165	.3861	.2716	.2349
	0.00170						.4467	.3472	.2539
405	0.00141	10.0	.4010 (350)	-.0287 (-25)	.4010 (350)	3.241	.3617	.2388	.3863
	0.00170						.3606	.2424	.6321

the spot size on the detector for best signal to noise ratio. Figure 32 shows a typical 3-lens Guoy Phase telescope design.

Table 39: Guoy Phase Telescope for 2-K interferometer.

Guoy Phase (Deg.)	*Waist at Detector (m)*	*Waist Slope at Detector (m/m)*	f_1 (m)	f_2 (m)	f_3 (m)	d_1 (m)	d_{12} (m)	d_{23} (m)	d_{34} (m)
450	0.00141	0.001	.3436 (300)	-.0287 (-25)	.6875 (600)	3.409	.3171	.3319	.6423
	0.00170						.3167	.3324	.9246
495	0.00141	0.001	.4010 (350)	-.0287 (-25)	.4010 (350)	3.510	.3891	.2789	.4901
	0.00170						.3877	.2745	.8343

Figure 32: Typical 3-lens Guoy Phase Telescope. Upper, beam profile, Lower, Guoy phase as function of distance from the Faraday rotator output port. The vertical line denotes the position of lenses.

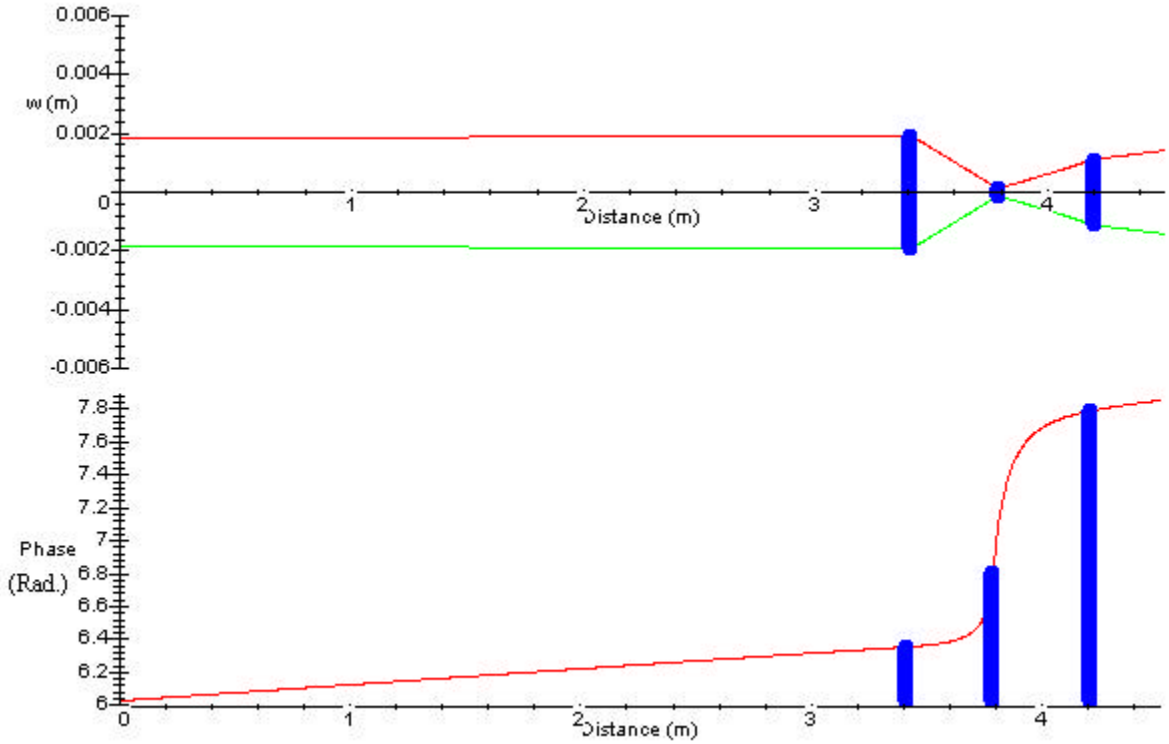

10 HIGH POWER COMPONENTS

Table 40 summarizes the results of the measurement and compare them with the requirement.

Table 40: Summary of measurement

item	*requirement*	*measurement*
Dynamic displacement by stray B-field of Faraday rotator (FR)	$4x10^{-9}$ m/Hz$^{0.5}$ (@1 Hz) $1x10^{-12}$ m/Hz$^{0.5}$ (@10 Hz) $3x10^{-23}$ m/Hz$^{0.5}$ (@100 Hz)	$1x10^{-12}$ m/Hz$^{0.5}$ (@1 Hz) $5x10^{-17}$ m/Hz$^{0.5}$ (@10 Hz) $6x10^{-28}$ m/Hz$^{0.5}$ (@100 Hz)
Vacuum contamination of FR (hydrocarbon pressure)	5×10^{-11} torr	9.4×10^{-12} torr
Power loss by FR thermal lensing	5%	3%
FR polarization	100:1	170:1
FR isolation	-35 dB	<-36 dB
Electro-Optical Modulator (EOM) residual intensity modulation	1×10^{-3}	$<2.5 \times 10^{-6}$
Alignment tolerance	4.3 deg	0.02 deg

10.1. Faraday Isolator

10.1.1. Stray B-fields

Because of seismic noise to the Faraday rotator (FR), the stray B-field leaking out from the FR's magnet fluctuates as a function of time, and thereby can disturb the operation of magnetic actuators used in nearby SOS's. The displacement of the SOS by this effect must be small enough to be compensated by the actuators. Our previous assessment based on calculated B-fields[1] indicates that the displacement of the closest SOS mirror due to this effect is smaller than the open-loop displacement of the mirror due to seismic noise, and therefore compensatable by the actuators. In this test, we confirm this conclusion using measured B-field.

A measurement of the stray B-field for three FR's is shown in Figure 33. All the FRs show very similar B_z for z<4 cm and the Synoptics FR shows an order of magnitude lower value for z>10 cm. The calculated B_z shows good agreement with B_z measured for the EOT FR.

1. S. Yoshida, R. Adhikari and D. Reitze, "Influence of the stray magnetic field generated by the Faraday isolator on SOS mirror actuators," LIGO T970149, 11/2/96

Figure 33: B_z measured along optical axis

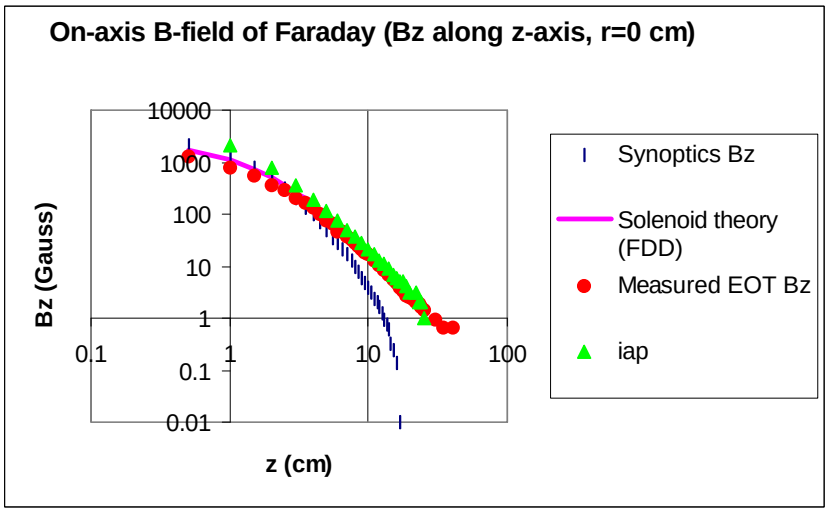

An estimate of the actual displacement expected for the mode cleaner mirror from these fields is shown in Figure 34. The FR is assumed to be located 25 cm away from the nearest SOS. This is a realistic distance from MC3 on HAM7 of 2K LIGO. In the whole frequency range of 0.01 - 100 Hz, all the displacement components are smaller than the open loop SOS displacement by two to five orders of magnitude.

Figure 34: SOS displacement estimated by measured B-field

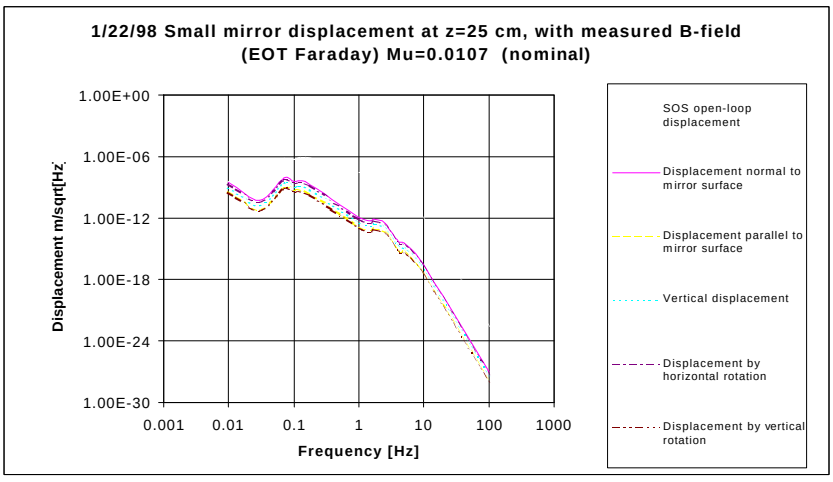

10.1.2. Vacuum Compatibility

The FI is located in vacuum. As such, it is subject to LIGO vacuum requirements for outgassing of hydrocarbon fragments. We selected an Electro-optics Technology custom-made FR for vacuum operation.

10.1.2.1 Requirements

The requirements for maximum allowed partial pressures of hydrocarbon products of with atomic masses in the 40 - 60 amu range is set at 5×10^{-11} torr (TBD SYS)

10.1.2.2 Measurements

Certification of the FR took place at the Caltech bakeout facility. The FR was first dissembled by removing the brass sleeve and TGG crystal within the bore of the magnet. The magnet and housing were baked separately from TGG crystal. Both were baked under the following conditions and with the following partial pressures:

Table 41: Bake Conditions for Faraday Rotator

Parameter	*Value*
Bake Temperature	60° C
Pump Speed	25 L/s

Table 42: Hydrocarbon Partial Pressures

Mass Number	*Partial Pressure*
41	3.8×10^{-12} torr
43	4.9×10^{-12} torr
53	2.2×10^{-13} torr
55	3.0×10^{-13} torr
57	1.4×10^{-13} torr
Total	**9.4×10^{-12} torr**

The total hydrocarbon partial pressure of **9.4×10^{-12} torr** meets the LIGO requirement. A second FR has been ordered to check these results.

10.1.3. Optical Testing

10.1.3.1 Requirements on the FR

SYS requires that the light from the PSL be coupled into the COC with 95% efficiency. When the TGG crystal of the FR is exposed to high power YAG radiation, it behaves as a focusing lens because of thermal lensing. This changes the wavefront of the YAG laser beam traveling toward the mode matching telescope and thereby degrades the coupling efficiency. This wavefront distortion cannot be corrected by the mode cleaner (MC) because the FI is placed after the MC.

Depolarization is required to be less than 100:1. The TGG crystal is a cubic crystal and is originally optically isotropic. However, when it is exposed to high power radiation, the thermal stress can generate birefringence and cause depolarization.

The isolation is required to be at the level of -70 dB by two Faraday isolators (FI). This means that the isolation level of one FI must be better than -35 dB.In this test, we measure the isolation ratio by measuring the double-pass depolarization of the FR.

10.1.3.2 Measurements

10.1.3.2.1 Thermal Lensing/Mode Quality

Thermal lensing studies were carried out for the FR manufactured by EOT. The waist sizes of the overlapping He/Ne probe laser and the YAG pump laser in the FR were respectively 1.79 mm and 1.62 mm. Figure 35 shows the thermal lensing observed at various YAG powers as a function of radial distance from the center of the thermal lens, r, normalized by the YAG waist size, w_{YAG}.The data were obtained by averaging the change in OPL measured for the same r over 360 degree around the center of the thermal lens.

Figure 35: Thermal lensing in FR (EOT) at various YAG powers

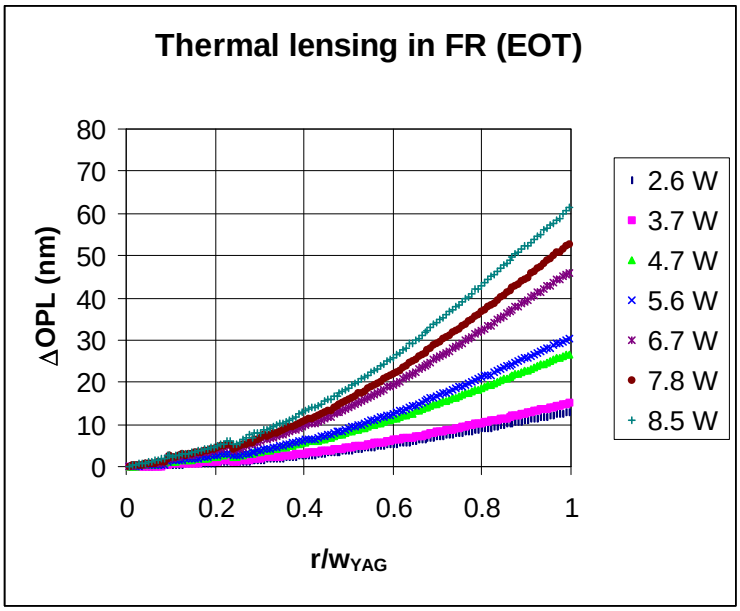

In Figure 36, we plot ΔOPL observed at the YAG waist as a function of transmitted YAG power. Because of the approximate linearity, this graph can be used to predict ΔOPL at higher powers. Also shown in Figure 36 are the results of the same ΔOPL measurement for a TGG rod of the same size without placing it in the FR magnet housing. The ΔOPL measured for the TGG rod placed in the FR magnet housing appears to be higher than the TGG only case. This discrepancy is possibly due to a change in thermal conductivity.

Figure 36: OPL change at YAG waist

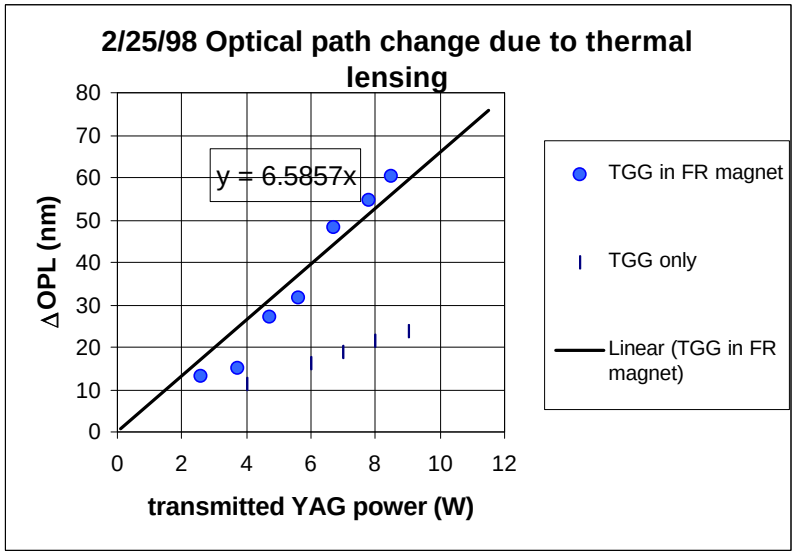

We next estimate the effective focal length of the observed thermal lens and compare it with the focal length that we calculated in PDR. To evaluate the effective radius of curvature of the thermal lens, we curve-fitted the observed ΔOPL to $\Delta OPL=r^2/2F$, where r is the radial distance from the thermal-lens-center and F is the effective focal length of the thermal lens. Since the w_{YAG} is the same as the actual beam radius of the 4K LIGO, the effective focal length obtained here represents the actual thermal lens of the 4K system. We next extrapolated Figure 36 on its YAG power axis to estimate ΔOPL at laser power higher than the maximum measured YAG power of 8.5 W. Using the value of ΔOPL determined in this a way and the formula $\Delta OPL=r^2/2F$, where r=1.62 mm, we evaluated F at several YAG laser powers. Figure 37 compares the effective focal length estimated in these fashions with the focal length calculated in PDR. Figure 37 also compares the effective focal length estimated by the ΔOPL measured using the TGG rod only. The effective focal lengths of the FR (TGG + magnet) based on the curve fitting and those estimated by the above-mentioned extrapolation show good agreement with each other, and both are smaller than the calculation in PDR by a factor of 2. Since the effective focal length for the TGG only case shows reasonable agreement with the PDR calculation, this factor of two discrepancy is possibly due to a change in thermal conductivity that occurs when the TGG rod is placed in the FR housing. Nevertheless, the presently estimated thermal lensing for the FR corresponds to power coupling loss of 3%. This is within the range of requirement, and can be improved by repositioning of the MMT mirrors 1, 2.

Figure 37: effective focal length of thermal lens

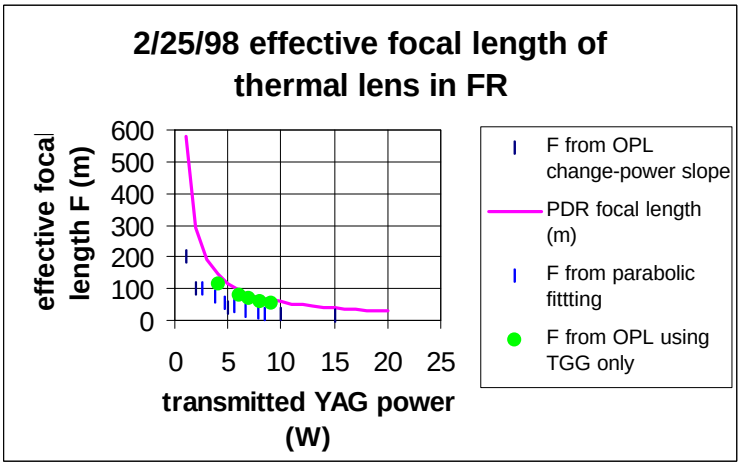

10.1.3.2.2 Depolarization in FR

Figure 38 shows depolarization P_t/P_i plotted as a function of P_i. Solid circles show P_t/P_i measured without the TGG rod, i.e., the background noise level of the setup. The measured depolarization shows clear quadratic dependence on P_i. This indicates that the observed depolarization is due to thermal birefringence of the TGG rod caused by the thermal load of the YAG laser. This is because the optical path difference due to thermally induced depolarization is proportional to P_i and the depolarization is proportional to the square of this optical path difference[1].

1. W. Winkler, A. Ruediger, R. Schilling, K. A. Strain and K. Danzmann, Birefringence-induced losses in interferometers, Opt. Comm., 112, 245-252 (1994)].

Figure 38: Depolarization in TGG crystal (EOT)

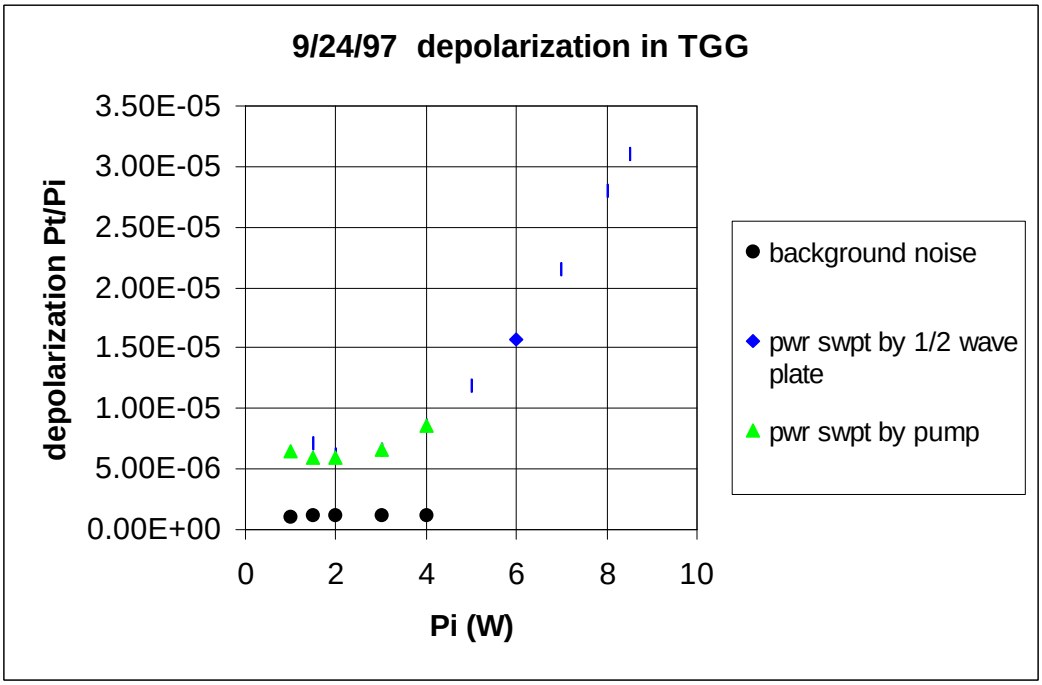

Figure 39 shows depolarization of the FR manufactured by EOT. It shows an order of magnitude higher depolarization than the case of the TGG crystal only.; however, it is sufficiently smaller than the targeted extinction ratio of 35 dB.

Figure 39: Single-pass depolarization of EOT

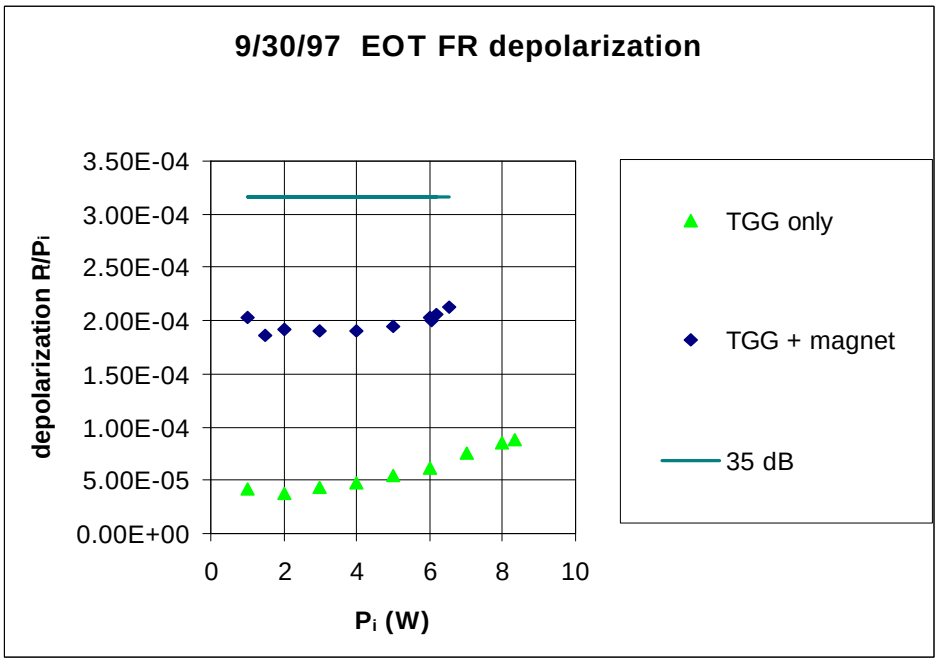

We also investigated the change in polarization state with temperature. The temperature dependence of the Verdet constant of the TGG results in change in the output polarization state. Figure 40 shows the influence of temperature change in depolarization. From our measurement *we find that the temperature change must be less than ± 3 deg to ensure 35 dB isolation.*

Figure 40: Change in depolarization due to temperature change (EOT). The solid line indicates 35 dB.

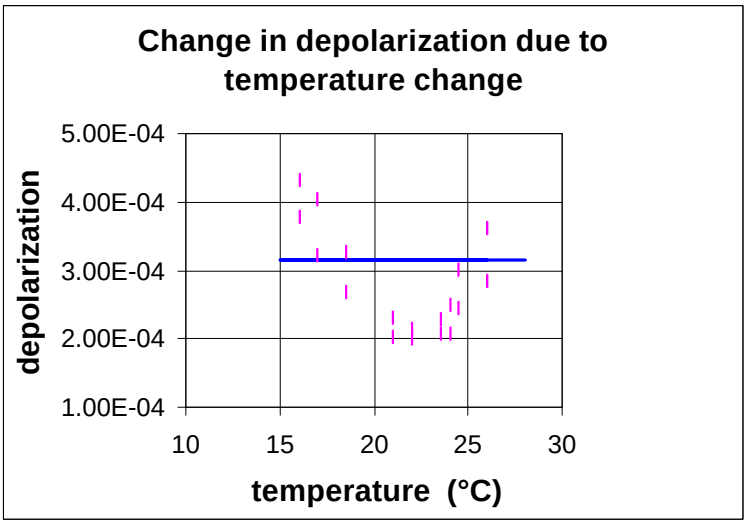

We investigated the dependence of the single-pass depolarization of the FR on its orientation with respect to the incident polarization. Figure 41 shows the result. We changed the relative angle between the polarization of the incident beam and the crystallographic axes of the FR by either rotating the incident polarization by a halfwave plate or by rotating the FR about the optical path. It is seen that depending on the angle, the depolarization can be different as much as an order of magnitude.

Figure 41: Angular dependence of EOT FR.

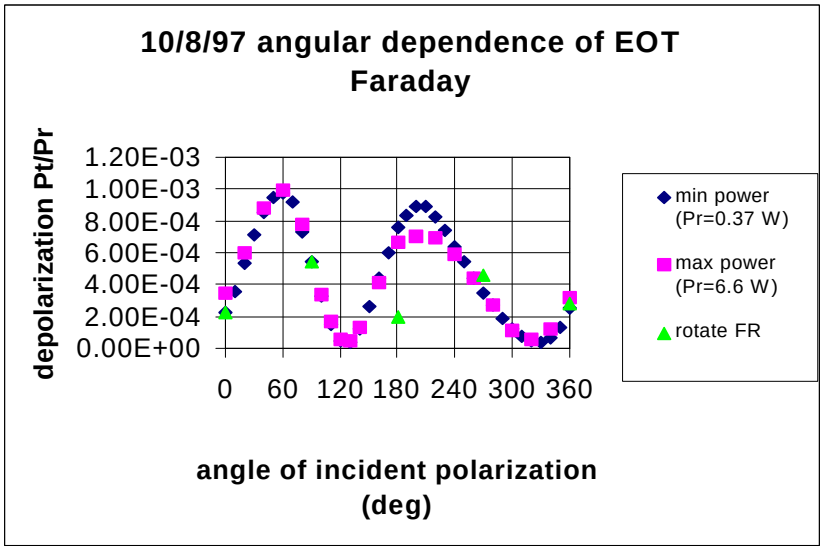

We next measured double-pass isolation using the same FR as Figure 39, after baking it at Caltech for a vacuum contamination test. In order to check if this baking degrades the performance, we first measured the single-pass depolarization. We adjusted the angle of the halfwave plate and the translational position of the FR with respect to the laser beam so that the single-pass depolarization might be minimized. The result is shown in Figure 42. No degradation by the baking is observed. We next measured the double pass depolarization P_{2r}/P_{2r} and defined it as the isolation ratio of the Faraday isolator (FI). For this measurement, we adjusted the angle of the halfwave plate and the translational position of the FR so that the double-pass depolarization might be minimized. The result is shown in Figure 42. The power dependence of the double-pass depolarization appears the same as the single-pass depolarization. At the maximum YAG power of 6.5 W, the isolation ratio is smaller than the targeted value of 35 dB by a factor of two (38 dB).

Figure 42: Double pass isolation of EOT FI

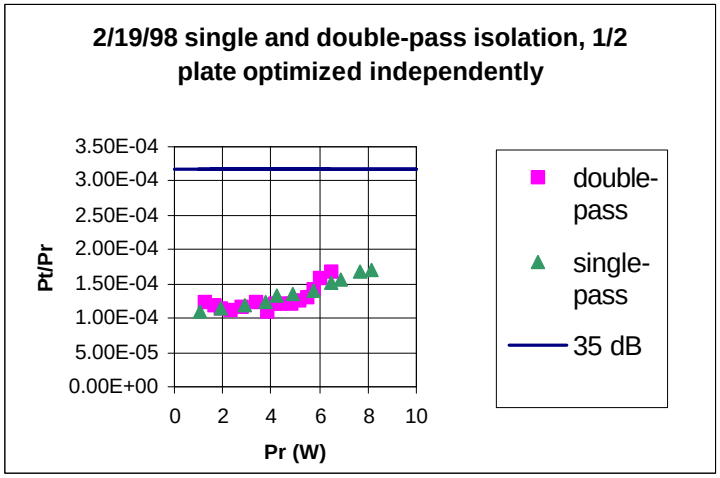

10.1.3.3 Faraday Isolator Selection (Type, Manufacturer, etc.)

Table 43 lists the specification of the Faraday rotator we have selected.

Table 43: FR specifications

Manufacturer	*Electro-Optics Technology*
Model Number	1845-12
Clear Aperture	12 mm
Transmission @ 1064 nm	>97%
Isolation @ 1064 nm	>30 dB

10.1.3.4 Polarizer Selection (Type, Manufacturer, etc.)

Table 44 lists the specification of the polarizer we have selected.

Table 44: FR specifications

Manufacturer	*CVI Laser Corp*
Model Number	CPAD-15.0-670-1064
Type	Glan Laser Double Escape Window Polarizer
Extinction ratio	5×10^5:1
Material	Calcite
Transmitted Wavefront	λ/4 at 633 nm
Antireflection Coating	All entrance and exit surfaces
Housing material	Black anodized aluminum
Damage threshold	cw 500 W/cm^2

10.2. EO Modulators

10.2.1. Requirements

10.2.1.1 Sideband Stability

10.2.1.1.1 Resonant SB

A residual amplitude modulation produced in an EOM causes a signal offset at the antisymmetric port. In order to make this offset negligibly small, the residual intensity modulation must be less than 10^{-3} [(1)]. Since the resonant SB has the largest modulation depth corresponding to the modulation index of 0.5, in this test we evaluate the intensity modulation around this modulation depth.

10.2.1.1.2 Nonres. SB

Same as Resonant SB.

1.P. Fritschel, G. Gonzalez, A. Marin, N. Mavalavala, D. Ouimette, L. Sievers, D. Sigg and M. Zucker, Length Sensing and Control Subsystem Preliminary Design, T970122-00D, 7/18/97

10.2.1.1.3 Mode Cleaner

Same as Resonant SB.

10.2.1.2 Damage Threshold/Thermal Lensing

When the laser beam is introduced to the EOMs, the power clipping must be lower than 10 ppm. For the EOM clear aperture of 2 mm, this corresponds to the beam waist of 0.4 mm. Thus the EOM must tolerate the corresponding power density. Thus in this test, we focus the 10 W YAG laser beam smaller than 0.4 mm and investigate if the $LiNBO_3$ crystal gets damaged.

10.2.1.3 Alignment Tolerance

The alignment between the angles of the EOM's axis and the incident polarization/the polarizer must be small enough to make the residual intensity modulation caused by RFAM be lower than the required value of $1x10^{-3}$. Table 45 shows the corresponding alignment tolerance.

Table 45: Required alignment tolerance

required RFAM (in intensity modulation)	*alignment tolerance*
1×10^{-3}	4.3 deg

10.2.2. Testing Results

10.2.2.1 Sideband Stability

Figure 43 shows the experimental arrangement for the measurement of the residual intensity modulation. The 10W YAG laser (Lightwave model 220-1064-10000) has at least three longitudinal modes that compete with one another causing instability in the frequency spectrum of the output beam. Therefore, we used a 700 mW-class NPRO type YAG laser (Lightwave model 220-1064-7000), which oscillates at a single longitudinal mode, as a probe laser for this measurement. To investigate the high power effect, we introduced the 10 W laser output with polarization orthogonal to that of the NPRO laser, so that it did not enter the photo-diode. The 10 W YAG laser beam was focused by a lens so that its radius at the EOM was the nominal value of 0.4 mm (10 ppm for the EOM aperture of 2 mm). Part of the beam was reflected by an optical wedge and was fed into an optical spectrum analyzer (Burleigh, model SA^{Plus}-200-XX) for monitoring the optical frequency spectrum The other part of the beam was fed into an RF photo-diode (EGG, FND-100) whose output was fed into an RF spectrum Analyzer (RFSA) and an oscilloscope, where the frequency spectrum and the total intensity were, respectively, measured. The EOM we tested was manufactured by New focus, Inc. (model 4003, broad band), and the modulation frequency was 21 MHz.

Figure 43: Experimental arrangement for sideband measurement.

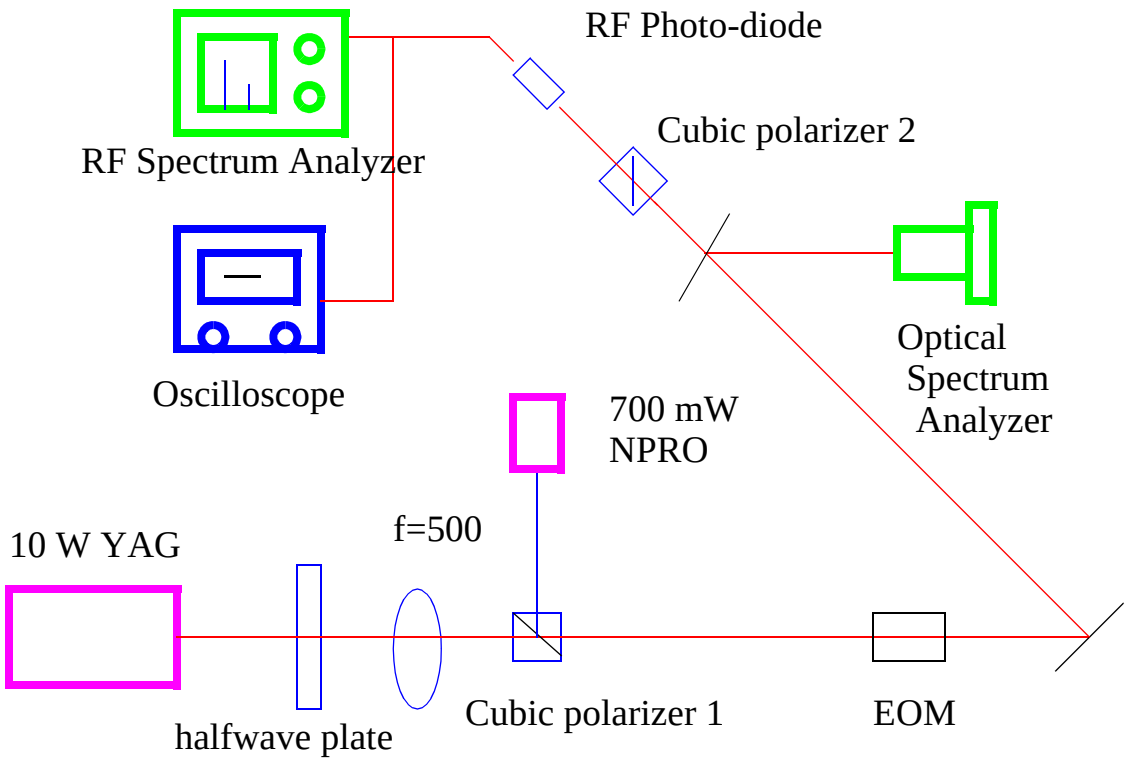

The residual intensity modulation is caused by misalignment of the angles between the incident polarization and the $LiNBO_3$'s crystallographic axis, and that between the $LiNBO_3$'s crystallographic axis and the orientation of the polarizer[1]. Depending on the initial phase retardation around which the modulation is applied, the intensity modulation observed in the RFSA has Ω component and 2Ω component at various ratios, where Ω is the modulation frequency. Thus in the following measurements, we monitored both components. In these measurements, the residual intensity modulation is evaluated as the ratio of the Ω (2Ω) component of the RFSA signal (called the ac term) to the total intensity measured by the oscilloscope (called the dc term).

- Temporal variation of the residual intensity modulation at 10 W
- Power dependence of the residual intensity modulation
- Residual intensity modulation at higher modulation depth

1.S. Kawamura, A. Abramovici and M. E. Zucker, "Improved multistage wide band laser frequency stabilization", Rev. Sci. Inst., Vol68, No.1, Pt.1, 223-229 (1997)

10.2.2.1.1 Temporal variation

After careful alignment of the angles between the $LiNBO_3$'s crystallographic axis and the initial polarization/polarizer orientation, we exposed the EOM to 10 W and monitored the residual intensity modulation for over 2 hours. The modulation index of this measurement was 0.4. Figure 44 shows the result. Over the whole observation period, the Ω and 2Ω components stay within ± 20%.

Figure 44: Temporal variation of residual intensity modulation

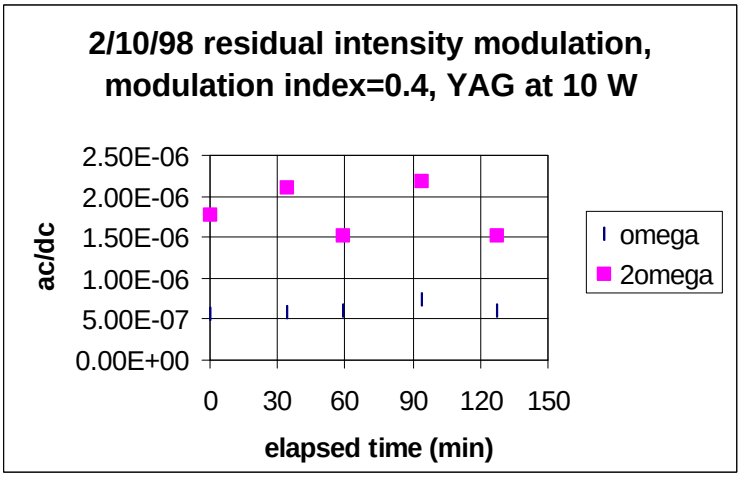

10.2.2.1.2 Power dependence

Figure 45 shows the influence of the superposed 10 W YAG laser power to the observed residual intensity modulation. The measurements were made after the $LiNBO_3$ crystal became thermally stable, which was checked by monitoring depolarization of the EOM (see below). *No substantial dependence on the YAG power is observed.*

Figure 45: Influence of YAG power to residual intensity modulation

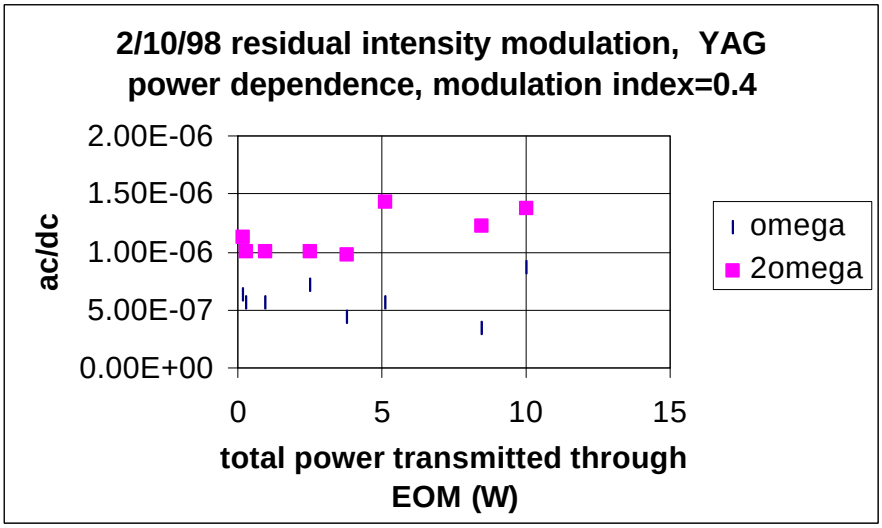

10.2.2.1.3 Residual intensity modulation at higher modulation depth

We also tested the residual intensity modulation at a higher modulation depth (modulation index = 1.1). This measurement was made after very careful alignment of the angles among the incident polarization, EOM's axis and the polarizer's orientation, and using the probe laser only. Figure 46 shows the result. The level of the intensity modulation is comparable to the case of the modulation index of 0.4.

Figure 46: Residual intensity modulation observed at a deeper modulation depth (modulation index=1.1)

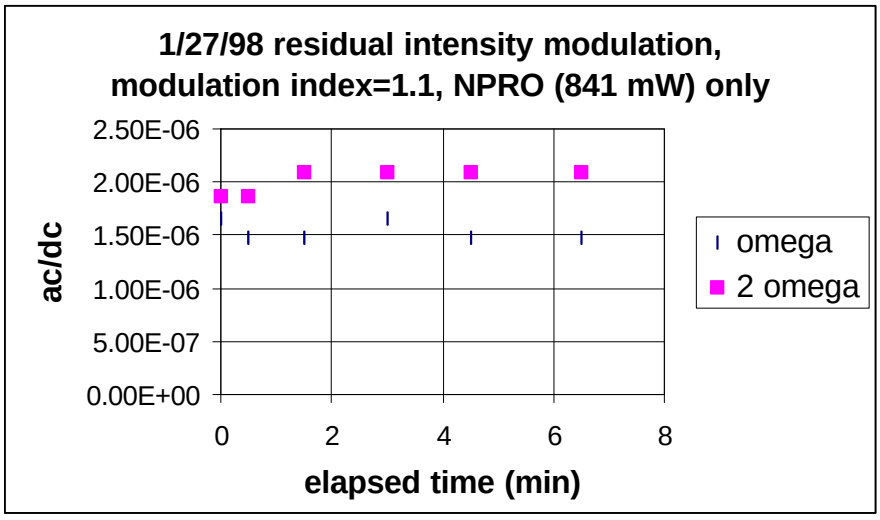

10.2.2.2 Damage Threshold/Thermal Lensing

We exposed the EOM to 10 W with the beam radius of 0.4 mm over 500 hours cumulatively. (The long-term exposure test is still ongoing). The transmission is a good indicator for a damage of the AR coating. So far, the initially measured transmission of 96±1% has not changed. Figure 47 shows power transmitted through the EOM as a function of cumulative exposure time.

Figure 47: YAG power transmitted through EOM

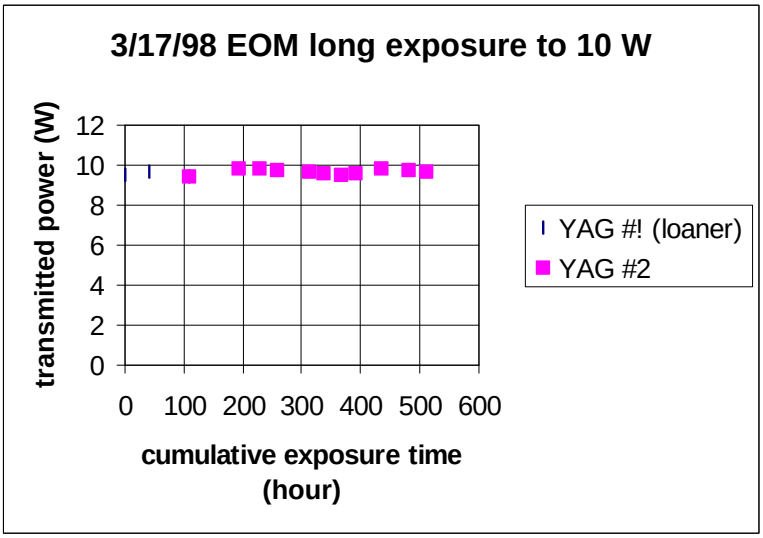

We measured thermal lensing in the EOM. Figure 48 shows thermally induced change in the optical path length in a $LiNBO_3$ crystal[1]. In this figure, the plots labeled as 3/20/98 are measurements made after cumulative exposure time of 528 hours and the plots labeled as Nov-97 are measurement made before the long exposure test. Both plots show the same OPL change indicating that the long exposure has not cause photo-refractive damage in the $LiNBO_3$ crystal.

Figure 48: Optical path length change by thermal lensing of EOM

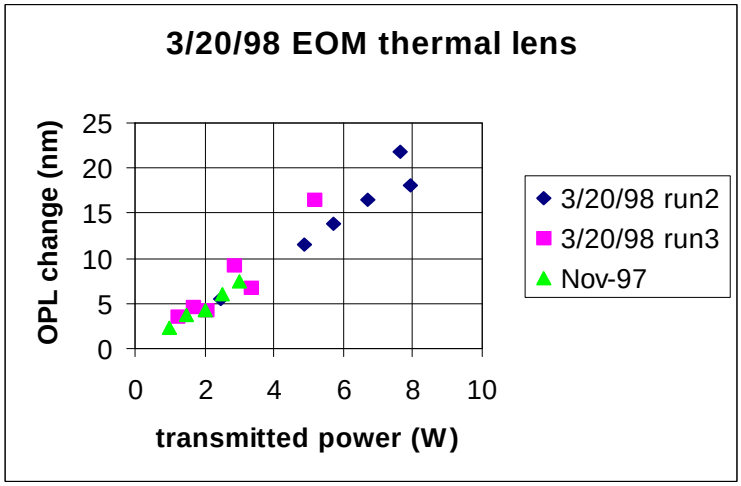

From the slope observed in Figure 48, the Optical path length change over the beam waist at 10 W can be estimated to be 24 nm. In the LIGO setup, the beam radius at the EOM is 0.4 mm. Thus the effective focal length F_{EOM} can be estimated from $F_{EOM}=r^2/2\Delta OPL= (0.4x10^{-3})^2/48x10^{-9}=3.3$ m. Since there are three EOMs in series, the overall thermal lens of the EOMs can be estimated approximately 1 m. This changes the waist of the beam after the EOMs from 0.397mm to

1. Part of this data was taken by J. Mansel in collaboration with Stanford University.

0.363 mm and shifts its location by 6.7 cm. These changes are compensatable by the mode matching telescope for the mode cleaner.

10.2.2.3 Alignment Tolerance

In order to make the intensity modulation lower than the required value of 10^{-3}, the misalignment in angle between the polarization and the EOM axis, and that between the polarization and the polarizer must be, respectively, less than 4 deg. Since this can be easily done, we examined how accurate we can align the angle. This was done by placing the EOM on a multi-axis stage having freedom of azimuthal rotation around the optical path, and monitoring the depolarization. Figure 49 shows the depolarization observed under the beast alignment we could achieve. Because of a random change in the ambient temperature, the depolarization varies as the time elapses going through multiples of phase retardation of 2π with an amplitude in depolarization of $1.5\text{x}10^{-7}$. The corresponding misalignment estimated from eq.(11) is 0.02 deg.

$$\left(\frac{E_h}{E_0}\right)^2 = \sin^2 2\theta \cdot \sin^2\frac{\delta}{2} \approx \frac{\delta}{2} \cdot \sin^2 2\theta \qquad (11)$$

where is E_h is the amplitude of the horizontal polarization (relative to the optical table) transmitted through polarizer 2, θ is the angle between the polarization and the fast axis

Figure 49: Depolarization in EOM at best alignment

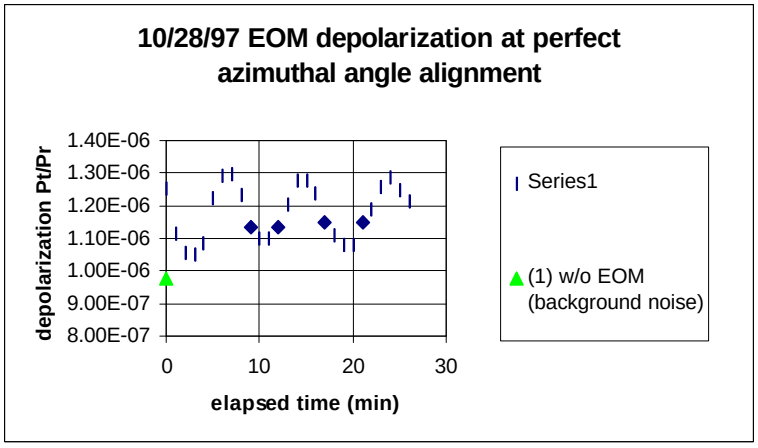

Table 46 compares this best alignment with the alignment tolerance for the required residual intensity modulation.

Table 46: Alignment tolerance and best alignment achieved

alignment tolerance	*best alignment achieved*
4.3 deg	0.02 deg

10.2.3. EO Modulator Selection (Type, Manufacturer, etc.)

Table 47 shows the specifications of the selected EOM.

Table 47: EOM specifications

Manufacturer	*New focus, Inc.*
Model #	4003
Wavelength	1.0 - 1.6 μm
Type	Resonant Phase Modulator
Operating Frequency	0.01 to 190 MHz
Modulation depth	0.1 - 0.3 rad/V @ 1 μm
Max Vπ	10 - 31 V @ 1 μm
Material	$LiNbO_3$
Max Optical intensity	1 W/mm^2 (1.3 1 μm)
Aperture	2 mm
RF Bandwidth	2 - 4% freq.
Impedance	50 ohm
Max RF Power	1 W